

1 **NOvA Test Beam detector calibration**

2 **Technical Note**

3 **Robert Kralik**

University of Sussex

4 October 2, 2023

5 **Abstract**

6 The NOvA Test Beam detector calibration uses the same calibration procedure as the
7 standard NOvA detectors. The main aim is to remove differences in energy deposition
8 within the detector and to provide an absolute energy scale from collected charge to phys-
9 ical energy units. This allows for a direct comparison of the deposited energy in the Test
10 Beam detector with the standard NOvA detectors. On top of that, the unique qualities of
11 Test Beam allow us to use the Test Beam calibration to validate the calibration process and
12 possibly to provide a simulation-independent absolute energy scale.

13 Contents

14 1 Introduction	3
15 2 Overview of the Test Beam detector	3
16 3 NOvA calibration process	7
3.1 Relative calibration	11
3.2 Absolute calibration	12
3.3 Calibration uncertainties	13
20 4 NOvA Test Beam detector calibration	13
4.1 Fibre Brightness	13
4.2 Simulation	14
4.3 Threshold and shielding corrections	15
4.4 Period 1	15
4.5 Period 2	19
4.6 Period 3	25
4.7 Period 4	31
4.8 Absolute calibration results	35
4.9 Results	35
4.10 Validation	35
31 5 Conclusion	50
32 References	50

33 1 Introduction

34 The NOvA Test Beam experiment aims to improve NOvA's sensitivity to the neutrino oscillation
35 parameters by improving our understanding of particle interactions and energy deposition
36 in the NOvA detectors, with the hope of reducing the total systematic uncertainty by about 10%
37 [1].

38 Specifically, Test Beam allows us to study the response of tagged single particles as a function
39 of their measured energies and compare it to the simulated prediction. It also enables us to
40 determine the energy resolution and the absolute energy scale of these particles. Additionally,
41 we are able to compare the response of beam and cosmic ray muons, to study fibre attenuation,
42 or to validate the entire NOvA calibration process. Test Beam detector was also equipped with
43 a combination of near and far detector readout electronics and filled with a variety of NOvA
44 scintillator oils, which makes it possible to make a comparison of their responses [2].

45 All the aforementioned benefits of running the NOvA Test Beam experiment require, or
46 benefit from, the Test Beam detector calibration.

47 The Test Beam detector calibration was first pioneered by Kevin Moulder who adapted the
48 NOvA calibration codebase for Test Beam and tested it on period 1 Test Beam data [3]. This
49 was followed by Anna Hall who improved it and got the first usable calibration of the Test
50 Beam detector based on the period 2 data [4]. Lastly, Rober Kralik took over and finished the
51 Test Beam calibration with all Test Beam data and a new simulation in 2023 [5].

52 2 Overview of the Test Beam detector

53 The NOvA Test Beam detector is a scaled down version of the near and far detectors shown on
54 figure 1. It is placed in the MC7b enclosure of the Fermilab Test Beam Facility in the path of
55 the MCcenter beamline with a variety of beamline detectors to measure and identify a range of
56 particles with various momenta [6].

57 The Test Beam detector started with commissioning runs in May 2019 and ran, with an
58 exception of regular summer shutdowns, until July 2022, after which it was decommissioned.
The Test Beam data periods are:

Period 1	March 22 nd 2019	- July 6 th 2019
Period 2	December 5 th 2019	- March 20 th 2020
Period 3	January 12 th 2021	- June 27 th 2021
Period 4	November 30 th 2021	- July 10 th 2022

Table 1: Test Beam detector data taking periods.

59
60 Majority of the Test Beam detector and its instrumentation is identical to the other NOvA
61 detectors, with a few exceptions that could have an impact on the calibration. We are going to
62 identify and discuss these differences in this section.

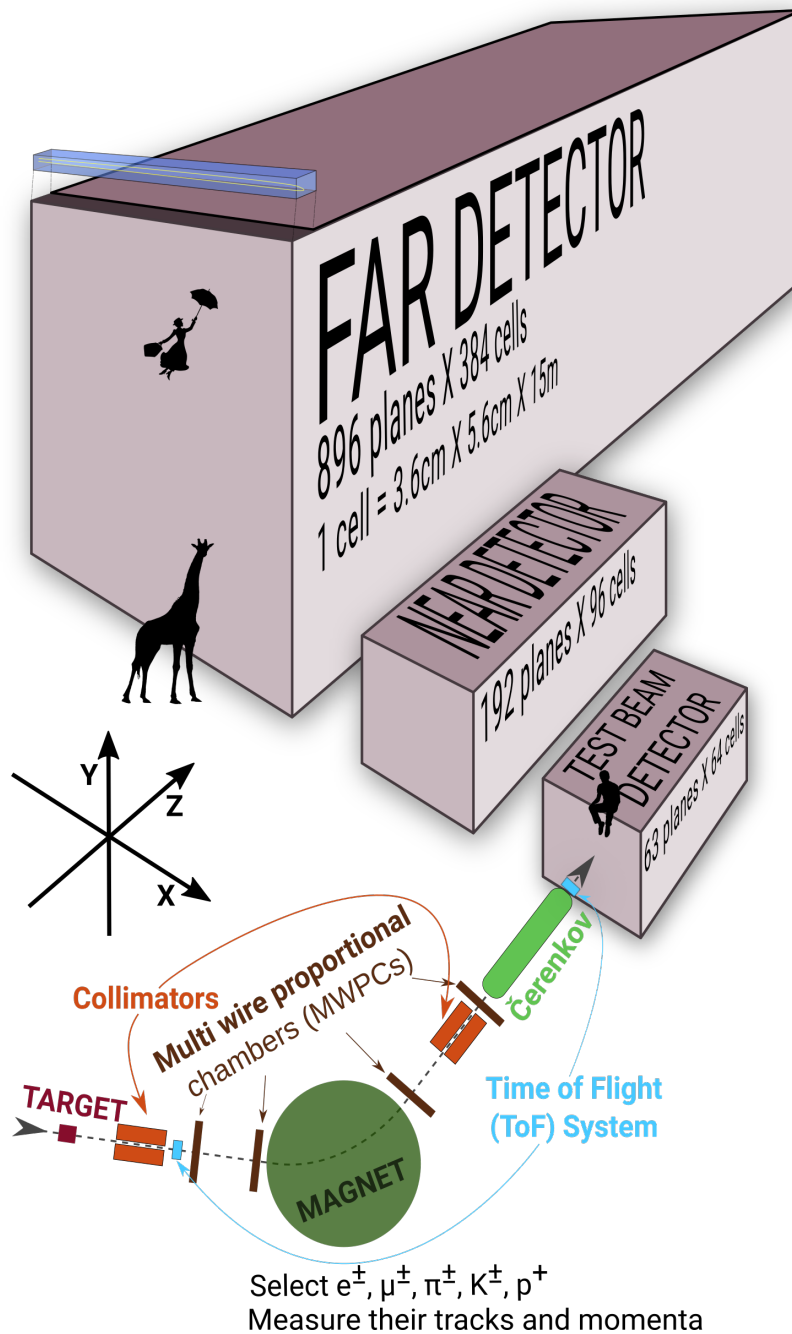


Figure 1: Comparison of Test Beam detector scale to the Near and Far NOvA detectors (and a man, giraffe, or Mary Poppins). Also shown are the Test Beam beamline detectors and components (not to scale), with arrows showing the direction of the beam. The three black arrows show the orientation of the detector coordinate system.

63 General parameters

- 64 The NOvA Test Beam detector consists of two 31-plane blocks, each beginning and ending
 65 with a vertical plane, with an additional horizontal plane glued in-between them to preserve
 66 the alternating pattern [7]. Each plane consists of 2 modules side-by-side, both made up of 32

67 cells. Each cell is 2.6 m long with an inner (without the PVC) depth and width of 5.9 cm and
68 3.8 cm respectively, same as for the other NOvA detectors. This brings the final dimensions of
69 the Test Beam detector to 63 planes \times 64 cells, or $2.6 \times 2.6 \times 4.1 \text{ m}^3$.

70 The 63 planes are numbered from 0 to 62, with even numbers corresponding to vertical
71 planes and odd numbers to horizontal planes. Cells are numbered 0 to 63, going from bottom
72 to top for horizontal planes and left to right, when facing the front of the detector, for vertical
73 planes.

74 The detector coordinate system is illustrated on figure 1. It is centred with (0,0,0) in the
75 centre of the first plane [8]. The x axis runs left to right when facing the front of the detector,
76 y axis bottom to top, and z axis goes along the beam direction from front to the back of the
77 detector. Position within each cell (w) is aligned with the x (y) axis for the horizontal (vertical)
78 cells, with $w = 0$ centred in the middle of each cell. The exact geometry of the Test Beam
79 detector was measured in several alignment surveys and is saved in gdml files [9].

80 In the past we encountered an issue when trying to align the Test Beam detector with the
81 beamline measurements by rotating the detector. This broke several assumptions within the
82 Test Beam geometry [8] and manifested as uncalibrated cells in the back of the detector [10].
83 This was fixed by realigning both the detector and the beamline separately, based on the last
84 alignment survey, measured during the decommissioning of the detector. We implemented the
85 fix in the production tag R23-04-05-testbeam-production.a [8].

86 Scintillator

87 The Test Beam detector is filled with several different versions of the NOvA scintillator oil,
88 which differ mainly in the way they were stored since the filling of the near and far detectors.
89 This is illustrated on figure 2.

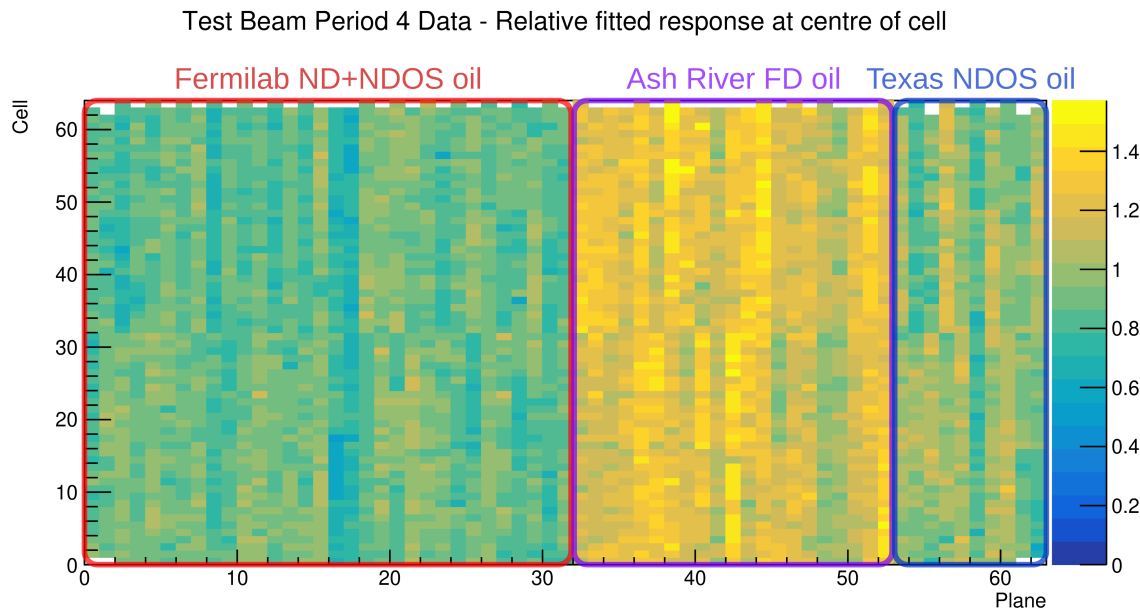


Figure 2: Uncorrected energy response in the centre of cells across the Test Beam detector showing a clear distinction between the different scintillator oils.

90 The original plan [11] was to use the scintillator from a tanker and one of the tanks located

91 outside at Fermilab. First tests showed acceptable results and the tanker oil was used to fill out
92 almost the entirety of the first block of the detector (first 32 planes) [12]. However, when we
93 loaded the oil from tank two into the tanker, it became extremely cloudy and unusable, possibly
94 due to contamination with water accumulated at the bottom of the tanks, which was mixed with
95 oil by the pump. The rest of the first block was topped up with high quality scintillator
96 from NDOS, which has been stored inside in barrels at MiniBooNE [1]. This is labelled as
97 "Fermilab ND+NDOS oil" on figure 2.

98 The first 21 planes of the second block (planes 32 to 52) were filled with the Far Detector
99 production scintillator shipped in from Ash River [13]. This oil has been stored in "totes" inside
100 a building and under several layers of black plastic [14]. We topped up these planes with the
101 NDOS scintillator [13].

102 The last 10 planes (planes 53 to 62) [13] were filled with scintillator drained from NDOS,
103 but stored in Texas A&M University and University of Texas at Austin [15, 16]. This scintillator
104 has higher light yield than the one from the tanker, but lower than the Ash River one [15].

105 In total the Test Beam detector is filled with 5418 gallons of scintillator oil with a weight
106 of approximately 28.6 tons [7].

107 **Readout**

108 The Test Beam detector uses in total 126 Front End Boards (FEBs), each reading out signal
109 from 32 cells (half of a plane) [7]. The readout is located on the top and right side (when
110 looking at the front) of the detector. 118 FEBs are version 4.1, same as in the Far Detector,
111 and 8 FEBs, located in pairs on planes 16, 17, 48 and 49, are version 5.2, same as in the Near
112 Detector. The Near Detector FEBs are designed to read out data in a faster rate and we used a
113 mix of FEB types to study the difference in their response and to validate both versions in the
114 same environment [17].

115 **Environment**

116 Unlike the near and the far detector, the Test Beam detector does not have any overburden to
117 shield it from cosmic particles, which affects their rate and energies inside the detector. There
118 is also less precise control of temperature and humidity than in the other detectors [source?],
119 which can potentially impact the scintillator and readout performance.

120 **Underfilled cells issue**

121 The Test Beam detector is slightly tilted around the Z axis by about 0.7° towards the readout.
122 This caused the top cells of both modules of all the horizontal planes (cells 31 and 63) to
123 be underfilled, creating an air bubble on the left side of the detector and severely affecting
124 the energy response in those cells [17]. This has been fixed [18] during the period 3 running
125 by adding extensions to the filling ports and overfilling the horizontal cells with the NDOS
126 scintillator stored.

¹²⁷ 3 NOvA calibration process

¹²⁸ Test Beam is following the same ideas and procedures as the standard NOvA calibration. This
¹²⁹ section intends to provide only a brief overview of the NOvA calibration. Further details can
¹³⁰ be found in the other NOvA calibration technical notes [19].

¹³¹ The purpose of calibration is to make sure that we get the same amount of energy wherever
¹³² or whenever it's deposited in whichever of NOvA's detectors and to express this energy in phys-
¹³³ ical units. The NOvA calibration uses cosmic ray muons, which provide a consistent, abundant
¹³⁴ and well-understood source of energy deposition and consists of two closely connected parts
¹³⁵ [20]:

- ¹³⁶ 1. The **relative calibration** corrects for attenuation of scintillator light as it travels through
¹³⁷ the cell to the readout, as well as for differences between detector cells.
- ¹³⁸ 2. This is followed by the **absolute calibration**, which only uses stopping muons when they
¹³⁹ are minimum ionising particles and calculates a scale between the measured charge read-
¹⁴⁰ out, corrected by the relative calibration, and the simulated energy deposition in physical
¹⁴¹ units of MeV. This scale is calculated for each time period and each detector separately,
¹⁴² which ensures the energy deposition is directly comparable wherever or whenever it oc-
¹⁴³ curred.

¹⁴⁴ There is also **timing calibration**, which corrects for the time differences of the signal to be
¹⁴⁵ processed and is done as a separate project to the relative and absolute calibrations and is out
¹⁴⁶ of scope of this technical note [21].

¹⁴⁷ The units and variables used to define energy deposited in NOvA detectors are listed in
table 2:

ADC	The digitized charge collected by the APDs from the Analog to Digital Converter [22].
PE	Number of Photo Electrons. Calculated by a simple rescaling of the best estimate of the peak ADC. The PE per ADC scale only depends on the FEB type and the APD gain settings. This is technically done before the calibration and serves as the base unit for calibration.
PECorr	Corrected PE after applying the relative calibration results. The correction is a ratio between an average energy response (a pre-determined semi-arbitrary num- ber) and the result of the the relative calibration fit (also called attenuation fit), which depends on w, cell, plane, epoch and detector. This makes the energy re- sponse equivalent across each detector.
MEU	Muon Energy Unit is the mean detector response to a stopping cosmic minimum ionising muon. Mean MeV/cm or mean PECorr/cm
MeV	Estimated energy deposited in the scintillator calculated from PECorr using the results of the absolute calibration. Additional correction for dead material needs to be made in order to get a calorimetric energy estimate.

Table 2: Definitions of variables commonly used in calibration [19, 20].

The final result of the NOvA calibration is the deposited energy in terms of physical units, which is in effect calculated as:

$$E_{dep}[\text{MeV}] = \underbrace{\frac{\text{MEU}_{truth}[\text{MeV}/\text{cm}]}{\text{MEU}_{reco}[\text{PECorr}/\text{cm}]}}_{\substack{\text{Absolute calibration} \\ (\text{Detector, epoch})}} \times \underbrace{\frac{\text{Average response}[\text{PECorr}]}{\text{Fitted response}[\text{PE}]}}_{\substack{\text{Relative calibration} \\ (\text{Detector, epoch,} \\ \text{plane, cell, w})}} \times \underbrace{\left[\frac{\text{PE}}{\text{ADC}} \right]}_{\substack{\text{Scale} \\ (\text{APD Gain, FEB})}} \times \text{Signal}[\text{ADC}], \quad (1)$$

where both the relative calibration results (blue fraction) and the absolute calibration results (red fraction) are stored in a database and applied together with the ADC-to-PE scale by the NOvASoft *Calibrator* package during processing of every hit in the NOvA detectors.

Creating calibration samples

To select good quality cosmic ray muons we first remove beam related events based on their time stamp relative to the time of the beam spill, as shown on figure 4. Then we apply basic reconstruction and track-based selection.

Since energy deposition in a cell depends on the path length the particle travelled through the cell, we only use hits for which we can reliably calculate their path length. We call these hits **tricell** hits, as we require that all accepted hits also have a recorded hit in both neighbouring cells of the same plane, as shown on figure 5. In case there's a bad channel in a neighbouring cell, we ignore this channel and look one cell further. We can then calculate the path length simply as the cell width divided by the cosine of the direction angle [19, 20].

For the absolute calibration we select muons that stop in the detector. For this we identify muons with a Michel electron at the end of their track and only selection those [23].

For each data period/epoch and each simulation version we create two calibration samples that are used as the input for the relative and absolute calibration. The samples are called [24]

- `pclist` = **list** of pre-calibrated hist; Contains all selected cosmic muon events and is used in the relative calibration;
- `pcliststop` = `pclist` files only containing stopping muons used for the absolute calibration

Fibre brightness

For data, the relative calibration is done for each individual cell in each plane to properly account for any potential variations. Therefore we have to repeat the attenuation fit $N_{cell} \times N_{plane}$ times. However, generating enough simulated events would be very computationally intensive. Additionally, we can assume that the simulated detector is approximately uniform plane to plane. Therefore, for simulation, we want to *consolidate* the detector planes and only consider variation in the two views and their cells, so repeat the fit $N_{cell} \times N_{view}$ times [25, 26].

There are some variations in the detector response cell by cell, that can be caused by different fibre brightnesses, but also by different qualities of the scintillator, air bubbles, APD gains, looped or zipped fibres and potentially others. To emulate these differences in the simulation without the need to simulate every cell individually and properly, we divide all the cells of

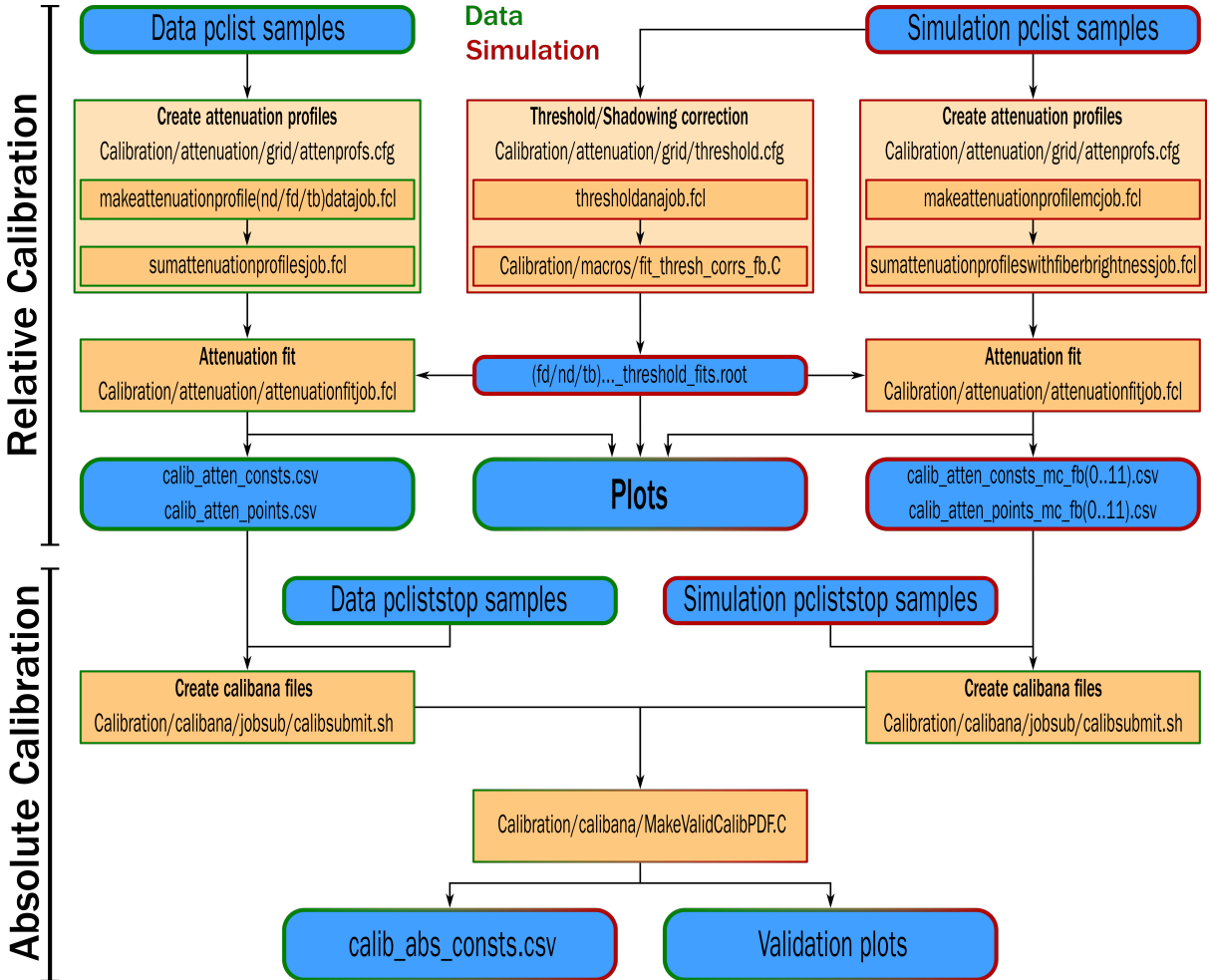


Figure 3: Flow chart showing the jobs (orange background) and files (blue background) needed and produced during the full NOvA calibration process. The left chain is showing the data calibration process (with green border) and is applied to every data calibration sample separately (periods or epochs). The center and right chains are showing the simulation calibration process (red border), which is redone only if there's a change to the detector simulation. The absolute calibration at the bottom combines data and simulation. The entire process is done separately for each NOvA detector.

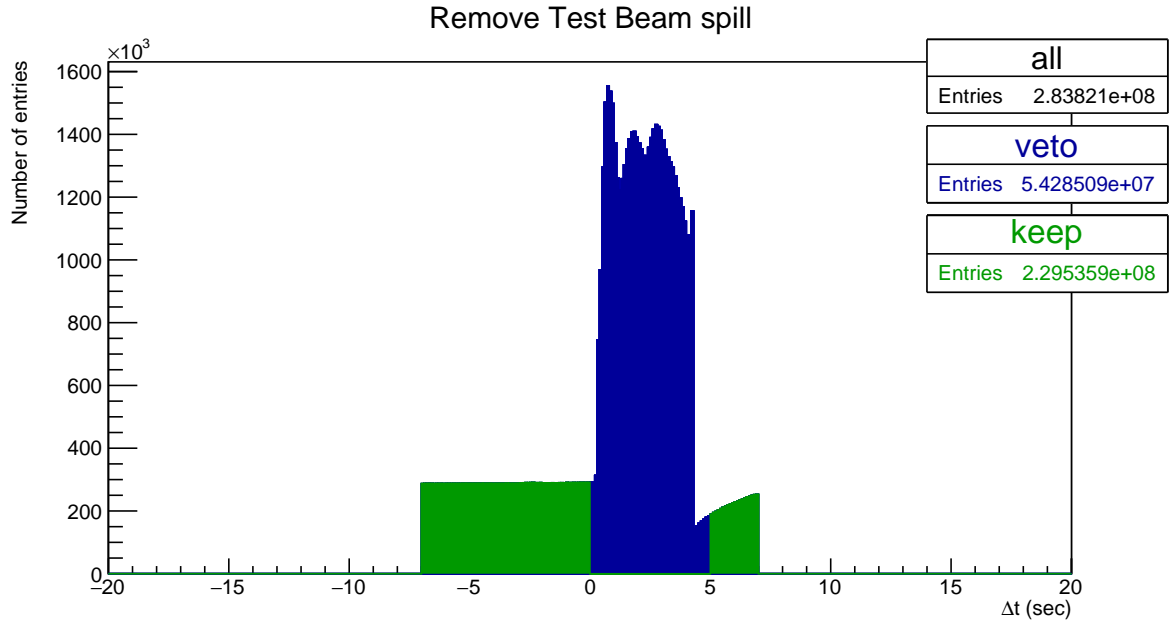


Figure 4: Test Beam beam spill events removed from the calibration samples. Test Beam beam spill is 4.2 seconds long and we remove events (in blue) within a 5 seconds window from the start of the beam spill. The remaining events (green) should mostly consist of cosmic particles. This example and the numbers of entries are for the full period 4 Test Beam sample.

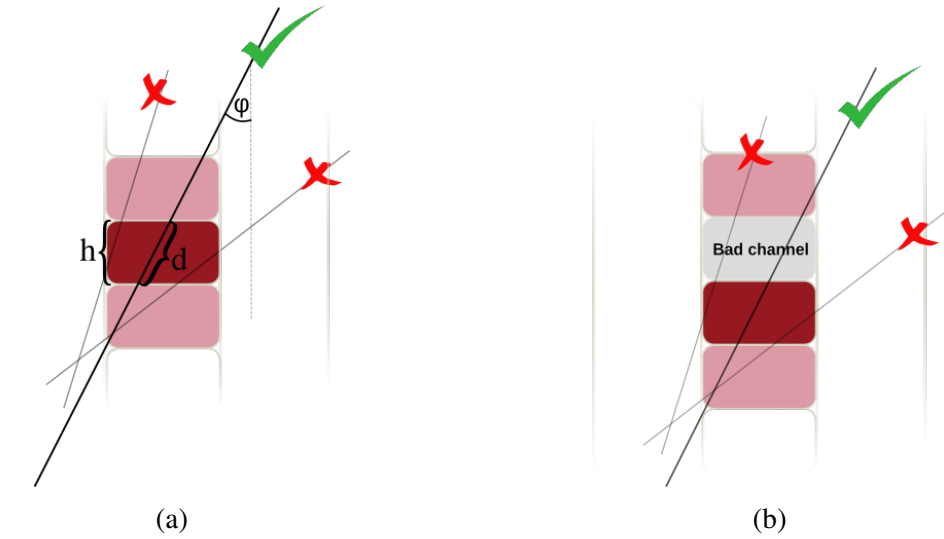


Figure 5: Illustration of the tricell condition (a). We only use hits that have two surrounding hits in the same plane to be used in the NOvA calibration. This is to ensure a good quality of the path length (d) reconstruction, which is calculated from the known cell height (h) and the reconstructed track angle (ϕ). In case the hit is next to a bad channel (b), we ignore this bad channel and require a hit in the next cell over.

each detector into 12 brightness bins, as shown on figure 6. These bins describe the relative differences in the detector response between individual cells [26]. Therefore in the end, for simulation we perform the attenuation fit in the $N_{view} \times N_{fiberbrightnessbin} \times N_{cell}$ phase space.

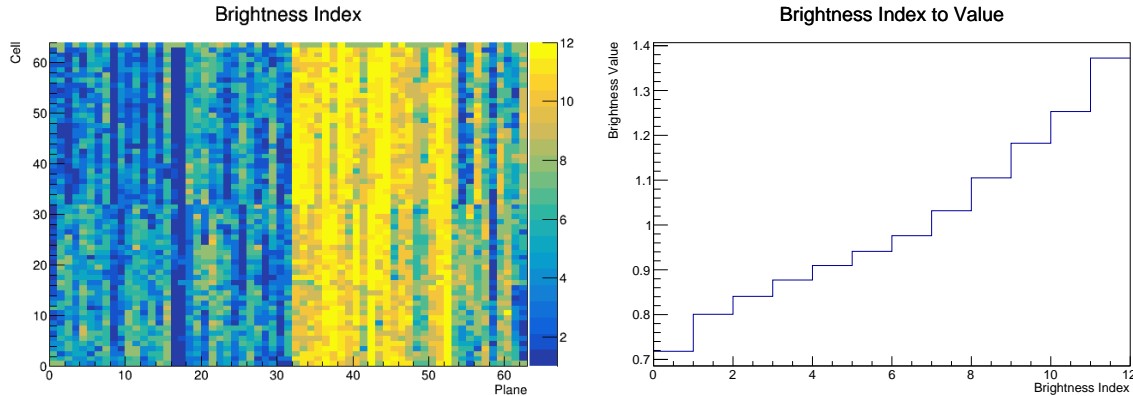


Figure 6: The Test Beam detector is (like the standard NOvA detectors) divided into 12 brightness bins (left plot), each representing a relative difference in energy response (right plot) due to different brightnesses of the fibres, scintillators, or readout.

TO DO: describe how do we create the brightness file

Threshold and shielding correction

Energy deposited far away from the readout may get attenuated enough to be shifted below the threshold. These low energy depositions would be missing from the attenuation fit, biasing it towards larger light levels going away from the readout. A similar effect, specifically for the vertical cells, is caused by using cosmic muons for calibration. The top of the detector effectively shields the bottom of the detector, skewing the energy distribution of cosmic muons. To correct for both of these effects, we use simulation to calculate the threshold and shielding (also called threshold and shadowing) correction by comparing the true and reconstructed information. We apply this correction before the attenuation fits [25].

3.1 Relative calibration

Relative calibration aims to create a fit, called *attenuation fit*, to the detector response over the position in a cell separately for every cell inside each detector. Scaling the fitted response to match the "average response" of the detector effectively removes relative differences throughout and between all cells across the entire detector. This average response is a single number chosen to approximately represent the average response in the middle of the cell. For the Far Detector this number is 39.91 PE, for the Near Detector it's 37.51 and for Test Beam it's the same as for the Far Detector 39.91. The scale of this number has no impact of this result as the absolute scale of the detector response is determined during the absolute calibration [20, 25].

To create the attenuation fit we follow the following procedure [20]:

1. Create *attenuation profiles*, which are profile histograms of detector response in terms of energy deposited per path length (PE/cm) as a function of position in the cell (w) through each cell for all planes. We construct the attenuation profiles over a little wider range

than the actual length of the cell and always with 100 bins for each detector. This means that smaller detectors, like the Test Beam detector, have a finer binning ($\sim 3\text{cm/bin}$) compared to the Far Detector ($\sim 18\text{cm/bin}$).

- 209 2. Analyse the attenuation profiles. The job to create the attenuation profiles also creates
210 validation histograms, which should be analysed prior to performing the attenuation fit
211 to make sure the attenuation profiles look as expected.
- 212 3. Apply the threshold and shielding correction that were created using the simulation plist
213 sample before the relative calibration.
- 214 4. Do the attenuation fit over the full length of each cell. The fit consists of
 - (a) exponential fit, which combines two cases. Light from the energy deposition travelling straight to the readout, or going the opposite direction, looping around the cell and then to the readout. The fitted function has a form:

$$y = C + A \left(\exp\left(\frac{w}{X}\right) + \exp\left(-\frac{L+w}{X}\right) \right), \quad (2)$$

215 where y is the response, L is the length of the cell and C , A and X are the fitted
216 parameters. X also represents the attenuation length.

- 217 (b) To remove the effect of residuals, mainly at the end of cells, we smooth out the
218 residuals from the exponential fit with LOcally WEighted Scatter plot Smoothing
219 (LOWESS).

- 220 5. Check the plots of the attenuation fit for a selection of cells.
- 221 6. Save the fit result to the database in the form of two csv tables. The *calib_atten_consts.csv* table
222 holds the results of the exponential fit, together with the final χ^2 of the fit. The
223 *calib_atten_points.csv* table holds the results of the LOWESS smoothing.

224 To ensure the quality of the attenuation fit, we only apply the results if the final $\chi^2 < 0.2$.

225 If $\chi^2 > 0.2$ we ignore the results for this cell and mark it as *uncalibrated*.

226 3.2 Absolute calibration

227 To find the absolute energy scale, we apply the relative calibration results on the stopping muon
228 sample and look at the energy they deposited in cells 1-2 meters from the end of their tracks.
229 In this track window they are minimum ionising particles and their energy deposition is almost
230 constant and well understood. We take a mean of their corrected deposited energy separate for
231 each view and for each calibrated sample. We then take the average over the two views to get
232 the final MEU_{reco}PECorr/cm for each sample [23].

233 From simulation we get the mean of the true energy deposited in scintillator MEU_{truth}MeV/cm
234 for the same sample of stopping muons. We ignore the energy that's lost in the dead material
235 (PVC extrusions) and deal with it separately. The absolute energy scale for each sample is then
236 the ratio of MEU_{truth}/MEU_{reco}. We save these absolute energy scales in another csv table called
237 *calib_abs_consts.csv* which stores the MEU values and their errors.

238 As part of the absolute calibration we also produce validation plots that show the effect of
 239 calibration on the distribution of the stopping muons. We analyse these plots and if everything
 240 looks all right load all the csv tables into the database.

241 **3.3 Calibration uncertainties**

242 WORK IN PROGRESS

243 **4 NOvA Test Beam detector calibration**

244 TO DO: list all the specific commands that need to be executed for the TB calibration. Like the
 245 coloured table in the data based simulation.

246 The calibration samples used for the Test Beam detector calibration are listed in table 3.
 247 We are using data from one of the Test Beam data-driven activity-based triggers. To produce
 248 these samples we (or production) use the [prod_tb_ddactivity1_pclist_job.fcl](#) FHiCL file from
 249 the novaproduct/novaproduct/fcl/testbeam repository, or the corresponding mc file.

250 The calibration samples were originally created in keep-ups by the production, but due to a
 251 fix to the Test Beam geometry, most of them had to be reproduced in 2023.

252 **4.1 Fibre Brightness**

253 To divide the Test Beam detector into fibre brightness bins we used the attenuation fit results
 254 for period 4 data (described in section 4.7), since that is the best detector conditions data we
 255 have. As we are only using the attenuation fit results in the centre of each cell, we've decided
 256 to allow some cells that initially failed the calibration, to be still used for the creation of the
 257 brightness file. As can be seen on figure 7, some attenuation fits have $\chi^2 > 0.2$, even though
 258 they correctly represent the energy deposition in the centre of that cell. By carefully investigating
 259 all cells with $\chi^2 > 0.2$ (possible for Test Beam, due to its small number of cells), we concluded
 260 it is safe to use all attenuation fit results, for which $\chi^2 < 0.7$.

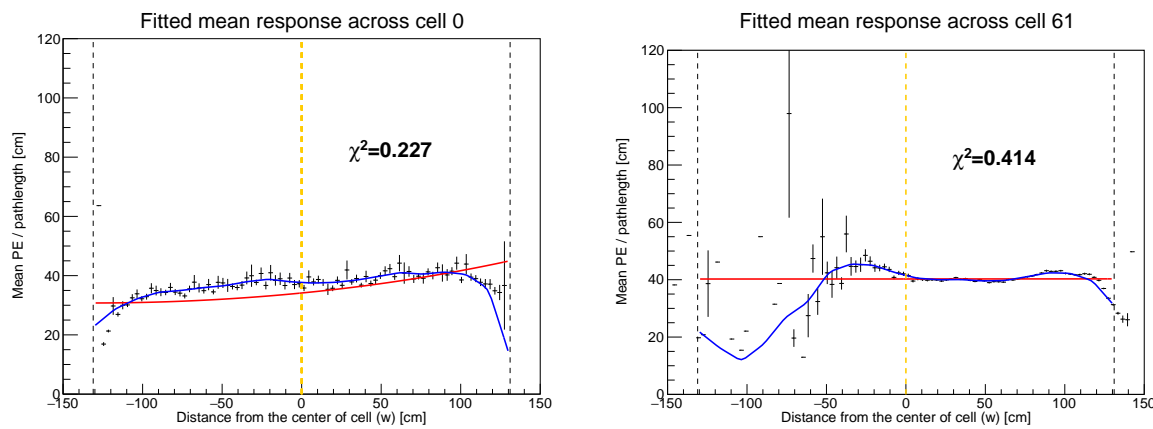


Figure 7: Attenuation fits for two cells that fail the calibration condition, but the fit (blue line) correctly represents the energy deposition in the centre of that cell (yellow dashed line).

pclist samples

Data period 2:

```
prod_pclist_R23-04-05-testbeam-production.a_testbeam_ddactivity1_period2_v1
```

Data period 3:

```
prod_pclist_R23-04-05-testbeam-production.a_testbeam_ddactivity1_epoch3a_v1
```

```
prod_pclist_R23-04-05-testbeam-production.a_testbeam_ddactivity1_epoch3b_v1
```

```
prod_pclist_R23-04-05-testbeam-production.a_testbeam_ddactivity1_epoch3c_v1
```

```
pclist_testbeam_detector_activity_epoch3d_R21-01-28-testbeam-production.a
```

```
pclist_testbeam_detector_activity_epoch3e_R21-01-28-testbeam-production.a
```

Data period 4:

```
prod_pclist_R23-04-05-testbeam-production.a_testbeam_ddactivity1_period4_v1
```

Simulation:

```
rkrilik_pclist_testbeam_databasedsim_R23-04-05-testbeam-production.a
```

pcliststop samples

Data period 2:

```
prod_pcliststop_R23-04-05-testbeam-production.a_testbeam_ddactivity1_period2_v1
```

Data period 3:

```
prod_pcliststop_R23-04-05-testbeam-production.a_testbeam_ddactivity1_epoch3a_v1
```

```
prod_pcliststop_R23-04-05-testbeam-production.a_testbeam_ddactivity1_epoch3b_v1
```

```
prod_pcliststop_R23-04-05-testbeam-production.a_testbeam_ddactivity1_epoch3c_v1
```

```
pcliststop_testbeam_detector_activity_epoch3d_R21-01-28-testbeam-production.a
```

```
pcliststop_testbeam_detector_activity_epoch3e_R21-01-28-testbeam-production.a
```

Data period 4:

```
prod_pcliststop_R23-04-05-testbeam-production.a_testbeam_ddactivity1_period4_v1
```

Simulation:

```
rkrilik_pcliststop_testbeam_databasedsim_R23-04-05-testbeam-production.a
```

Table 3: SAMWEB definitions of the Test Beam calibration samples.

261 4.2 Simulation

262 We used a data-based simulation of cosmic muons for the Test Beam detector calibration. The
263 details are described in the Data-based simulation of cosmic muons (not only) for calibration
264 technical note [link to docdb]. We used half of period 4 data (used every second event as saved
265 in the root file, therefore sampled from the entire period 4) as inputs and the newly created fibre
266 brightness file to inform the simulation on the realistic detector conditions.

267 The distribution of events cosmic muon events from the new simulation is shown on figure
268 8.

269 The results of the attenuation fit are shown for each cell (in its centre) on figure 9. The
270 blank cells show which cells failed the attenuation fit (their $\chi^2 > 0.2$). Most of the uncalibrated
271 cells are on the edges of the detector, which is expected as those have much fewer events that
272 pass our selection than the rest. Examples of a standard detector response and of the response
273 for cells on the edge of the detector are shown of figure 10.

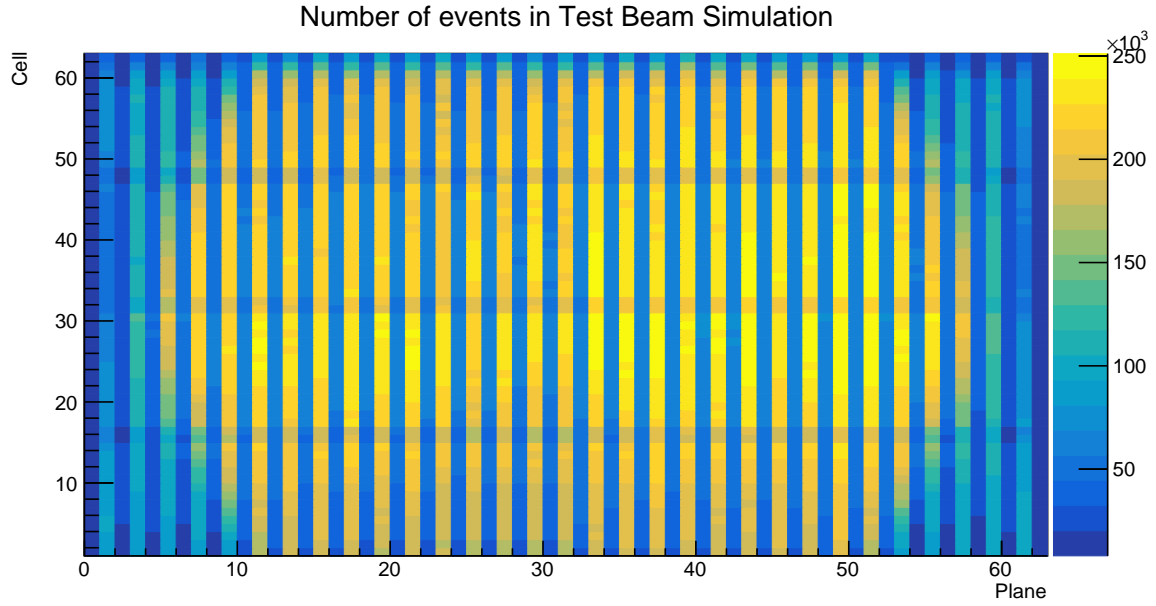


Figure 8: Distribution of events in the Test Beam simulation calibration sample.

(I should explain here what is on the plots maybe - red is the exponential fit and blue is the total with with the LOWESS. Most cells have the expected response of slow rise towards the readout falling down on the edges).

There is only one cell in the middle of the detector that is left uncalibrated, which is the cell 32 in a vertical plane in the brightness bin 5, shown on the top right of fig. 10. The corresponding $\chi^2 = 0.227$. It seems the reason the $\chi^2 > 0.2$ is an exceptionally high response with a large uncertainty in the last bin.

This is a much better result of the relative calibration (attenuation fit) for a simulation than the previous versions of Test Beam detector calibration simulations were able to accomplish.

4.3 Threshold and shielding corrections

The threshold and shielding correction for Test Beam is almost uniform across all cells as can be seen on figure 11. This is expected as the height of the Test Beam detector is 2.6 m has only a negligible effect on the energy distribution of cosmic muons or on the threshold saturation. The correction is basically just a normalization factor, except for the cell edges, but there is a large variation in the energy response there anyway due to low number of events. Since the relative calibration only cares about relative differences across the detector, a normalization factor doesn't change anything.

4.4 Period 1

TO DO: add a description of period 1 data

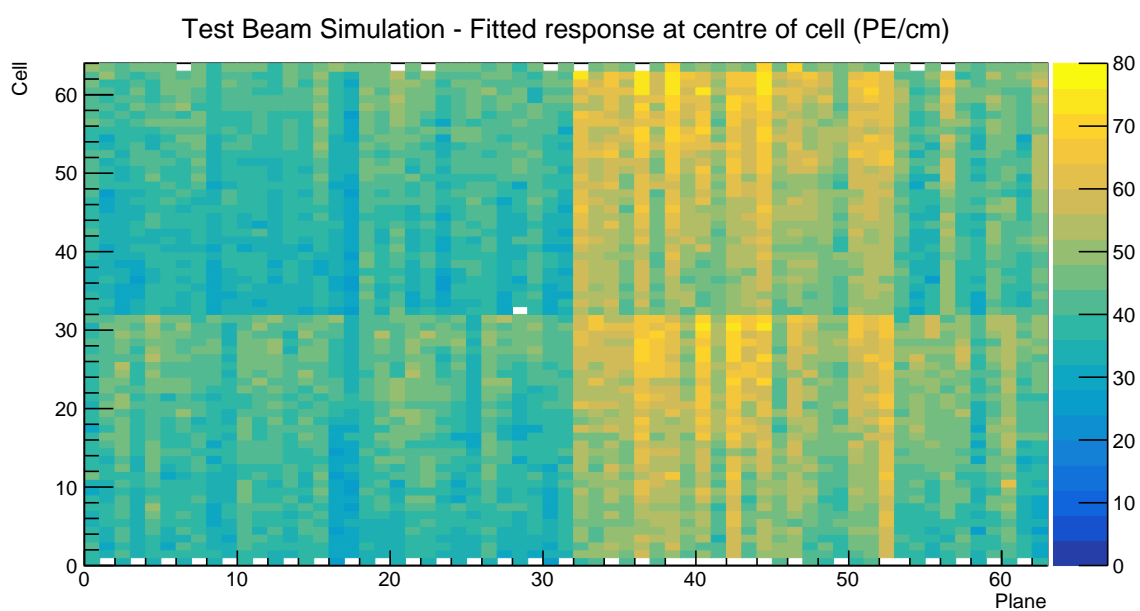


Figure 9: Overview of the attenuation fit results for the Test Beam detector calibration simulation. Each cell represents the result of the attenuation fit to the energy response in the centre of that cell. The blank cells are uncalibrated.

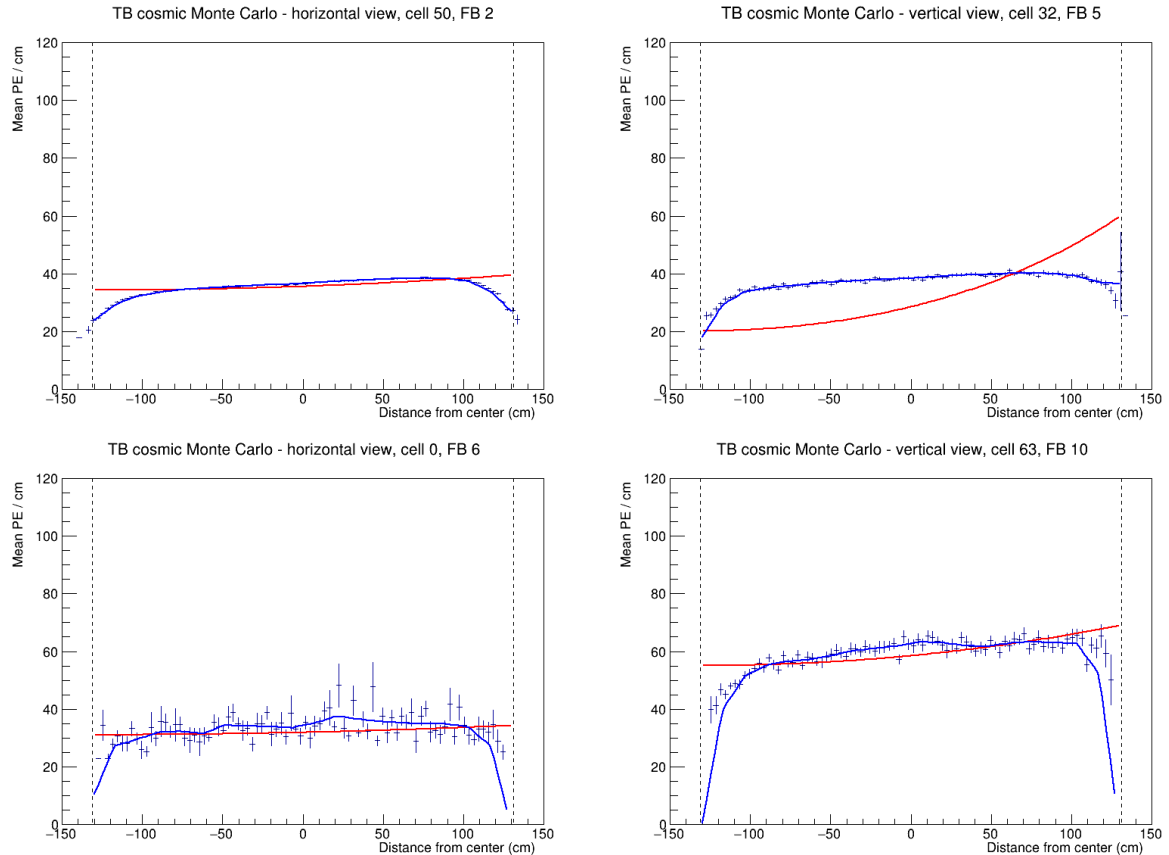


Figure 10: Attenuation fits for a selection of cells in the Test Beam calibration simulation. Top left is an example of a successful attenuation fit, top right is a failed fit due to statistical fluctuation in the last bin and the bottom plots show failed fits for cells on the edges of the detector.

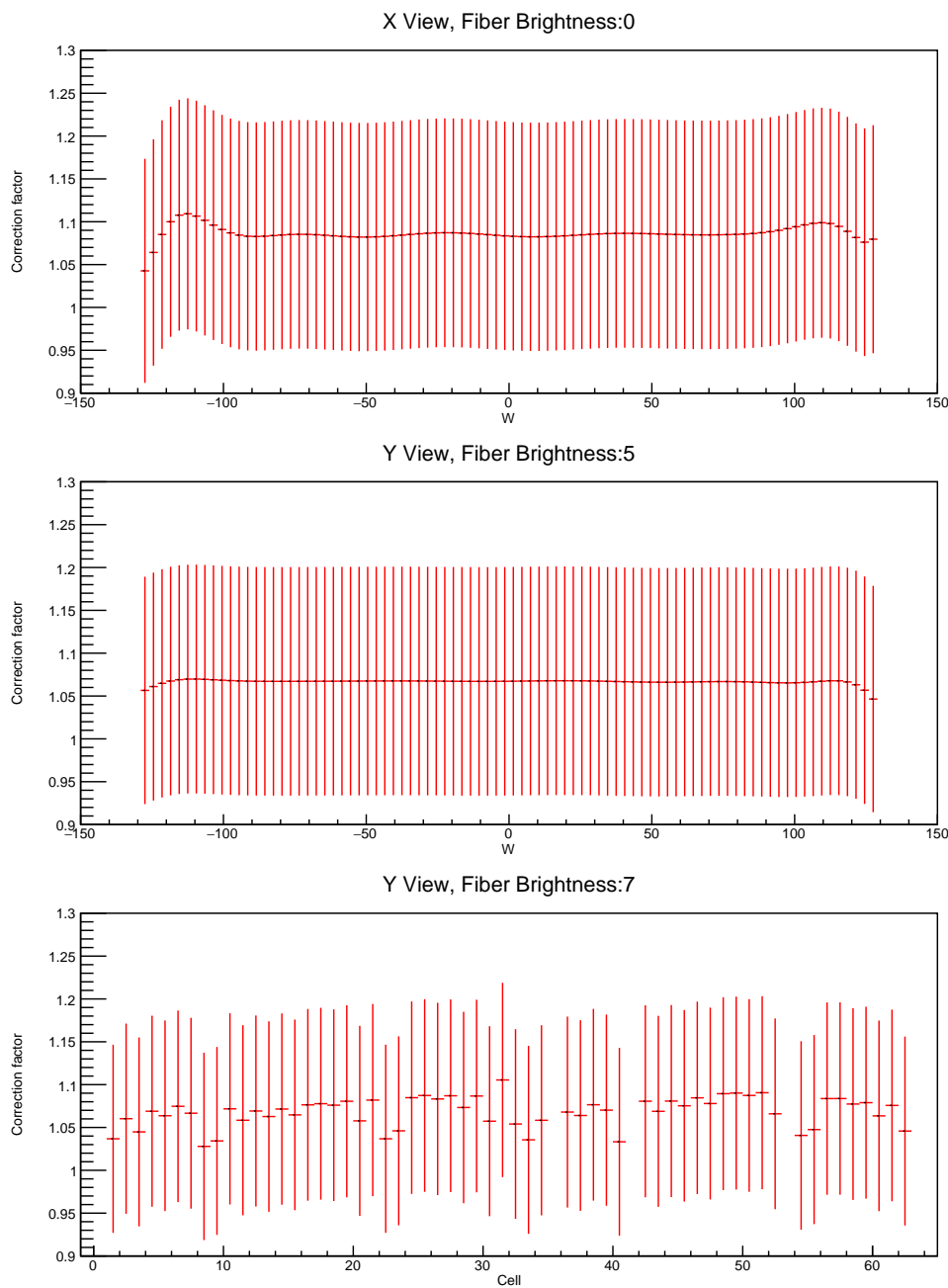


Figure 11: Examples of threshold and shielding corrections for the Test Beam detector

293 4.5 Period 2

294 The underfilled cells issue described in section 2 was present throughout period 2 data taking.
 295 This can be clearly seen on figure 12, represented by the empty cells 31 and 63 in the horizontal
 296 planes, which were marked as bad channels and therefore ignored during processing. This also
 297 affects the neighbouring cells to the underfilled cells, which have fewer events due to the tricell
 298 condition.

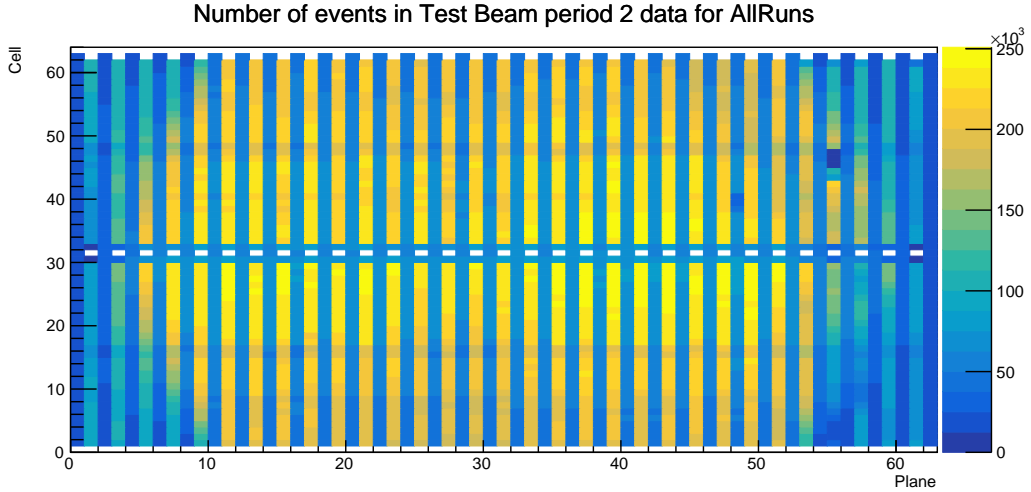


Figure 12: Distribution of events in the period 2 Test Beam data calibration sample.

299 There was also an issue of switched cables from the readout in plane 55 between cells 3
 300 and 46 [27], which can also be seen on figure 12. This is manifested as fewer total number of
 301 events in those cells and in their neighbours, again due to the tricell condition.

302 Officially, period 2 is divided into 6 epochs 2a - 2f, compared on figures 13, 14 and 15. The
 303 epochs mostly differ in the use of various FEB firmwares, with epoch 2c being a trigger study
 304 with paddles. As can be seen on the plots, the individual epochs vary only slightly, only in a
 305 small normalization. We decided to use the entire period 2 without splitting it into any smaller
 306 samples for calibration.

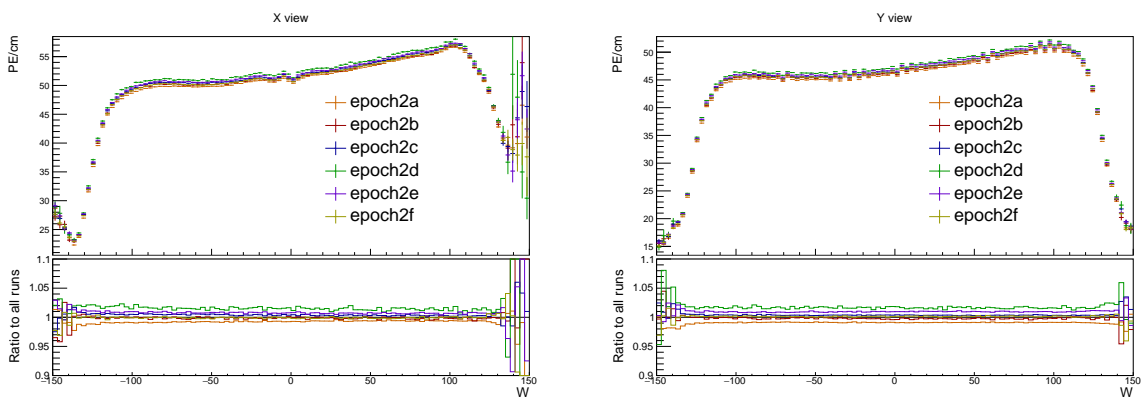


Figure 13: Uncorrected average energy response as a function of the position within a cell (w) for epochs in period 2. It is clear that there is no significant difference between the various epochs.

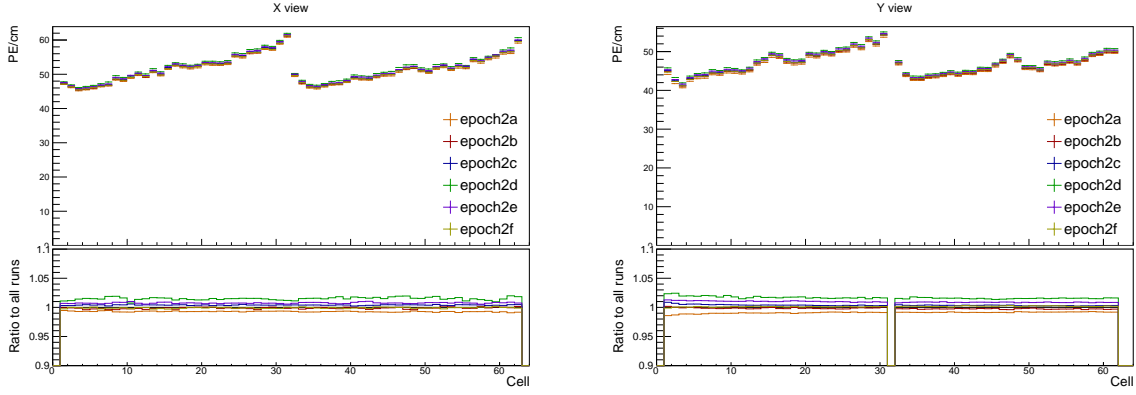


Figure 14: Uncorrected average energy response as a function of cells for epochs in period 2.

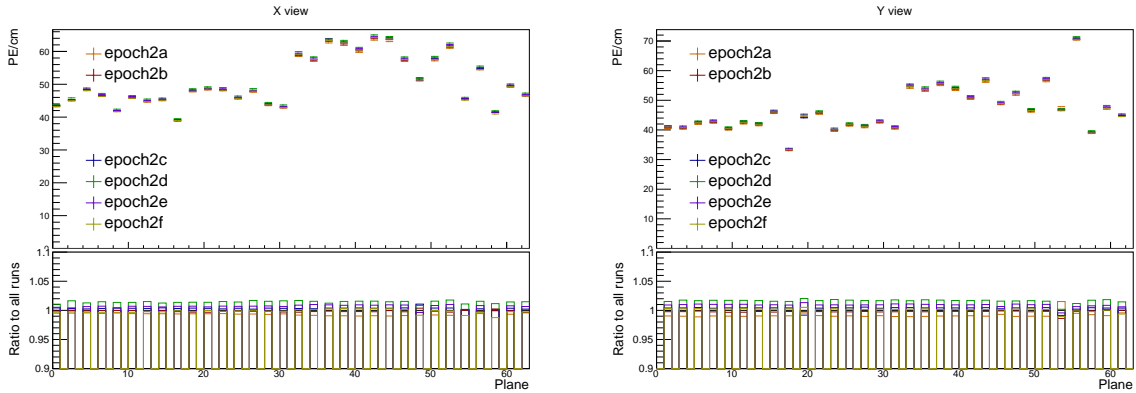


Figure 15: Uncorrected average energy response as a function of planes for epochs in period 2.

307 Period 2 relative calibration results

308 The results of the attenuation fit for period 2 are summarised on figure 16 showing the fitted
309 response at the centre of each cell, or blank cell if the cell failed calibration.

310 Most of the cells have the expected response, as shown on the left plot of figure 17. Here
311 the mean response in PE/cm slowly and approximately constantly rises towards the readout
312 (right side of the plot) and drops down on the cell edges, marked with dashed lines.

313 Some cells have a non-flat response across the cell, with one or more regions with lower en-
314 ergy response, as shown on the right plot of figure 17. These low regions are (almost certainly)
315 a real physical effect caused by zipped, or possibly even twisted fibres [28], present in all of
316 NOvA's detectors. Relative calibration corrects for this effect in data, but zipped fibres are not
317 included in simulation, for any of the detectors. This could potentially cause issues with the
318 ADC threshold in simulation.

319 Since the underfilled cells were marked as bad channels we didn't even attempt to calibrate
320 them. Their neighbours have fewer events due to the tricell condition but majority of them
321 pass the calibration condition, as shown on figure 18. The neighbouring cells in plane 1 don't
322 pass the calibration due to low statistics and therefore large fluctuations, as shown on figure 19.
323 This is likely due to a combination of the tricell condition and plane 1 being on the edge of the
324 detector, which typically has fewer (accepted) hits than the center as shown on figure 12.

325 The left half of plane 55 has $> 3 \times$ larger response than it's surrounding planes, as shown

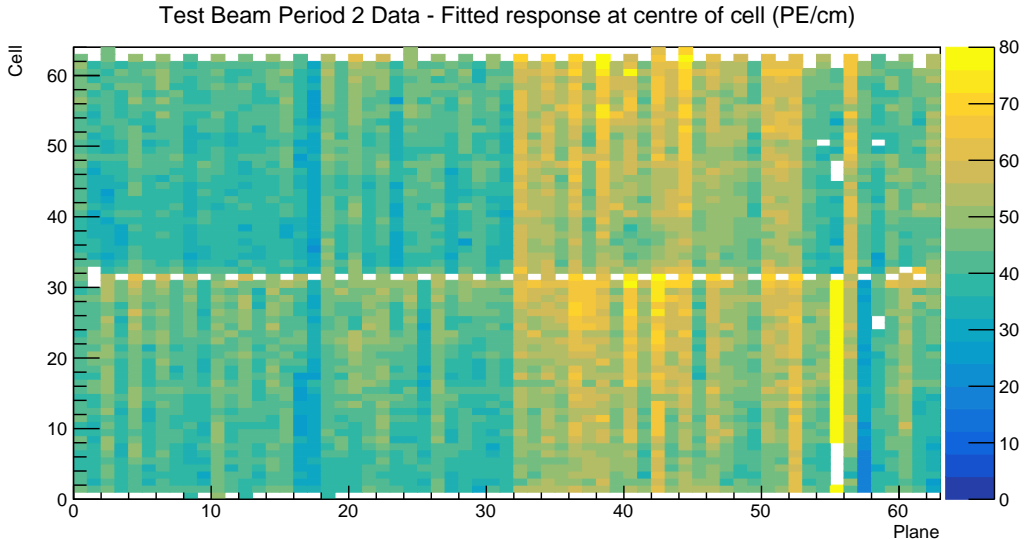


Figure 16: Overview of the relative calibration results for the Test Beam detector period 2 data. Each cell represents the result of the attenuation fit to the energy response in the centre of that cell. The blank cells are uncalibrated.

326 on the left plot of figure 20. Similarly, the left half of plane 57 has lightly lower response than
 327 the surrounding planes, as shown on the right plot of figure 20. This is due to the corresponding
 328 APDs/FEBs faultily recording different energy response than the real energy deposited in the
 329 detector. Since this is present for all data, not only for the cosmic muons used for calibration,
 330 it is important to correctly calibrate them. The issue can arise if these FEBs have been "faulty"
 331 only for a limited time of the entire calibrated period. Since we are doing the attenuation fit on
 332 the profile histograms, if an FEB records a standard response for half of the time and $7\times$ larger
 333 response for the seconds half, calibration is going to assume the response was $4\times$ larger the
 334 entire time, which is incorrect. Since both of these planes are in the back of the detector, we
 335 decided to ignore this effect for period 2.

336 The swapped cables in plane 55 have almost no events, which affects both them and their
 337 neighbours as shown of figure 21.

338 Several cells in the end of the Test Beam detector are uncalibrated due to bins on the edges
 339 of the cell having an unusually high response, or no events at all, as shown on figure 22. It is
 340 unknown if this is a real physical effect, possibly related to the fibres, or unfiltered noise hits,
 341 or something else entirely. Since these cells are in the end of the detector, it is safe to ignore
 342 them.

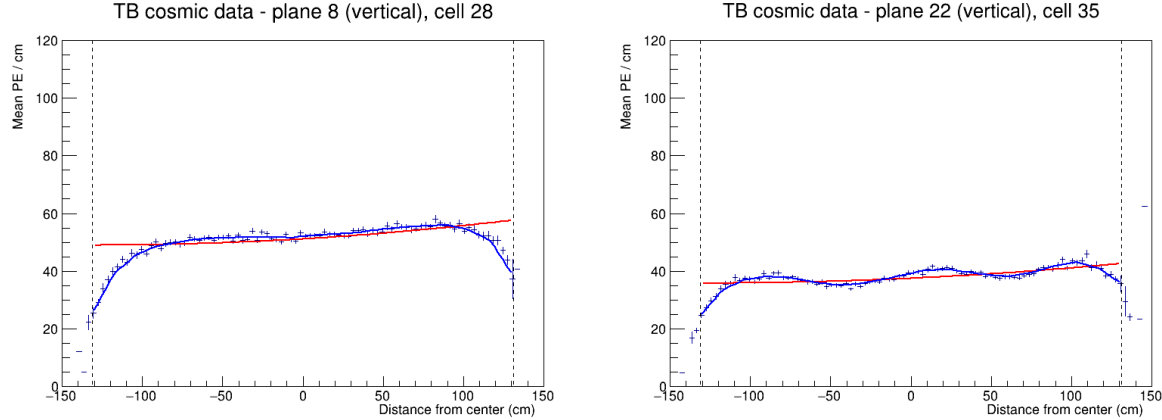


Figure 17: Attenuation fits for a selection of cells in period 2. Left plot shows an example of the standard energy deposition in the Test Beam. Right plot shows the effect of zipped fibres.

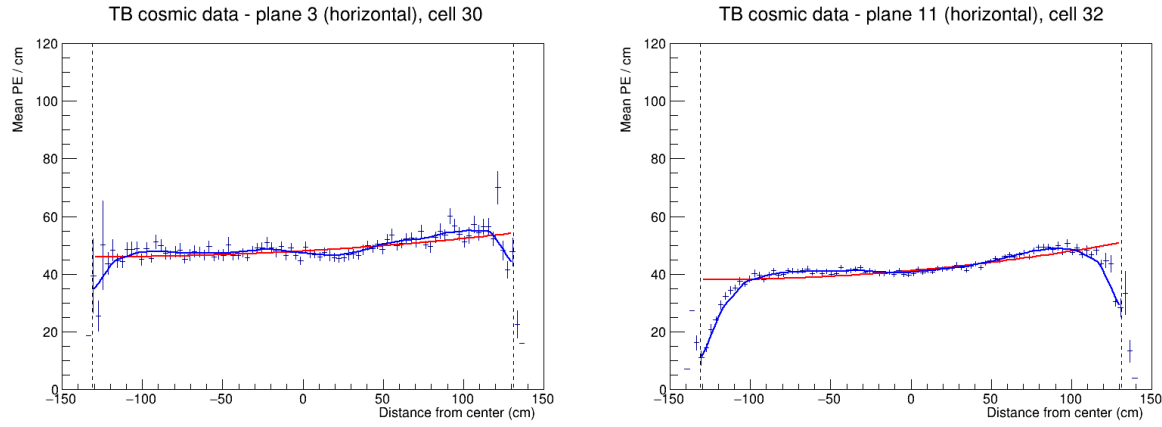


Figure 18: Fit to the energy response in period 2. The cells neighbouring the underfilled cells have fewer events and therefore larger fluctuations than the "usual" Test Beam cell.

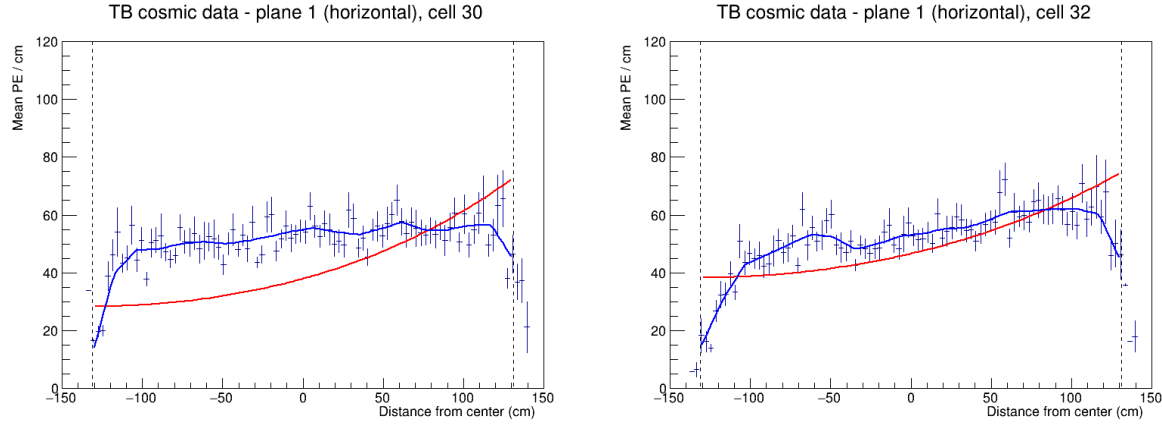


Figure 19: Fit to the energy response in period 2. The neighbouring cells to the underfilled cells in plane 1 are uncalibrated due to low statistics.

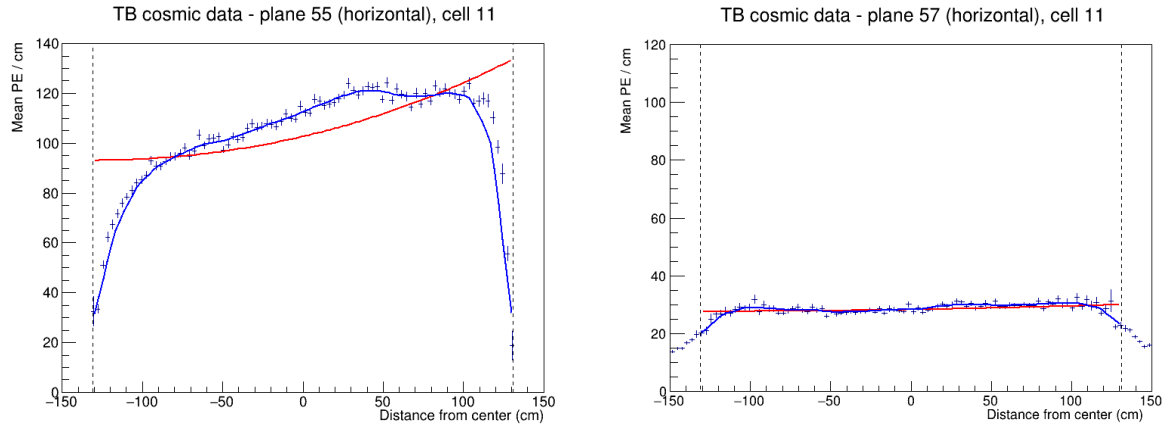


Figure 20: Fit to the energy response in period 2. Lower halves of planes 55 and 57 have a different scale of energy response than the surrounding planes.

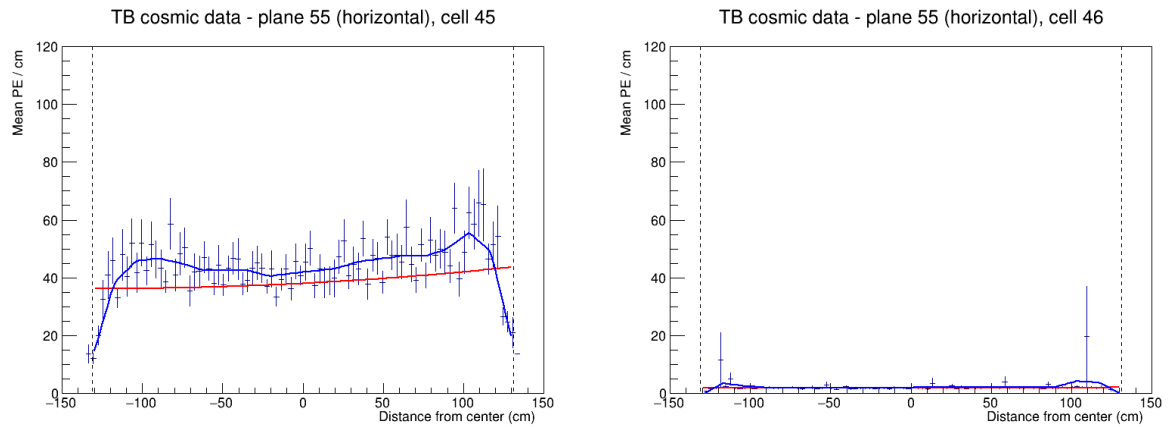


Figure 21: Fit to the energy response in period 2. Cells with swapped readout cables have almost no recorded events as shown on the right plot. This also affect their neighbouring cells due to the tricell condition as shown on the left plot.

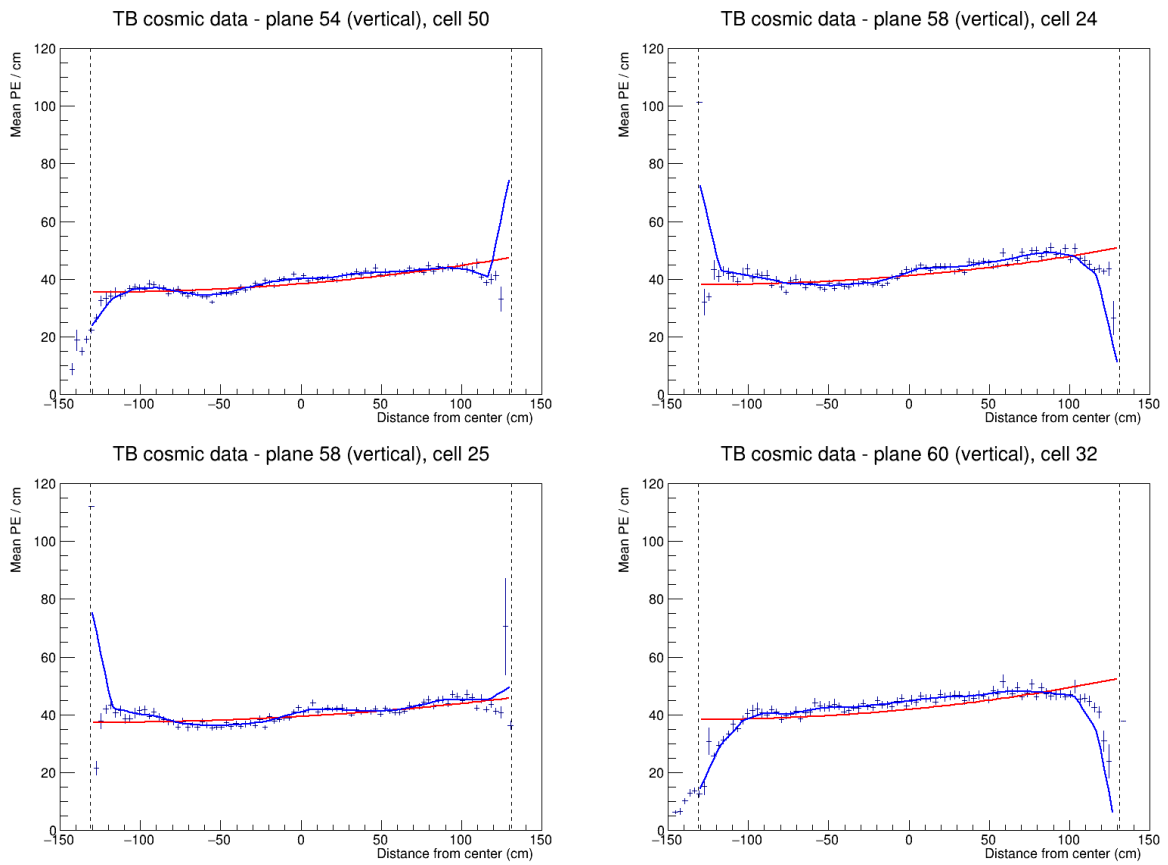


Figure 22: Fit to the energy response in period 2. Examples of cells that have an unusually high or low energy response at the edge of the cell. These cells are not calibrated.

³⁴³ **4.6 Period 3**

³⁴⁴ The underfilled cells were refilled (or overfilled) during the period 3 data taking. This was the
³⁴⁵ main motivation for dividing period 3 into individual epochs as shown on table 4. One more
³⁴⁶ major event that could impact the Test Beam data is the replacement of several faulty FEBs,
³⁴⁷ which motivated the creation of epoch 3e.

Epoch 3a	January 12 th 2021	Underfilled cells
Epoch 3b	April 21 st 2021	Overfilling the back 9 horizontal planes and the 7th horizontal plane from the front
Epoch 3c	April 27 th 2021	Overfilling of the 15 front horizontal planes (except the 7th, which was already done) and the 14th horizontal plane
Epoch 3d	April 30 th 2021	Overfilling of the remaining 8 horizontal planes
Epoch 3e	May 12 th 2021	FEB swaps

Table 4: Test Beam period 3 epochs, their start dates and the reason for their separation.

³⁴⁸ The refilling of the underfilled cells can be clearly seen on the cell hits distribution on figure
³⁴⁹ 23 and on the distribution of energy deposition across horizontal cells (Y view) on figure 25.

³⁵⁰ From the cell hits distributions we can also see there are a few channels (cells) that were
³⁵¹ likely dead for a certain time and weren't recording the same number of events as the surround-
³⁵² ing cells. This is specifically plane 48, cell 39 in all of period 3 and plane 18, cell 31 in epochs
³⁵³ 3d and 3e.

³⁵⁴ The energy distributions across vertical cells and planes (X view) on figures 25 and 26
³⁵⁵ shows, that the top half of plane 58 has a very distinctly different energy deposition compared
³⁵⁶ to the rest of the cells, while having the same number of events, as can be seen on figure 23.
³⁵⁷ This is the most impactful of the faulty FEBs replaced for Epoch 3e.

³⁵⁸ From these discussion, we have decided to calibrate epochs 3a, 3b and 3c together (all
³⁵⁹ epochs containing any underfilled cells) and separately calibrated epochs 3d and 3e. The faulty
³⁶⁰ FEB in plane 58 is far enough in the back of the detector that we didn't find it necessary to
³⁶¹ calibrate epochs 3d and 3e separately. Also epochs 3b and 3c only contain a few days worth of
³⁶² data, which wouldn't be enough for a successful attenuation fit.

³⁶³ **Combined epochs 3a, 3b and 3c relative calibration results**

³⁶⁴ The results of the attenuation fit are summarised on figure 27 showing cell × plane distribution
³⁶⁵ of the fitted response at the centre of each cell.

³⁶⁶ We can see that some of the underfilled cells that have been refilled for epochs 3b or 3c are
³⁶⁷ now calibrated thanks to including them into the same attenuation fit. An example of energy
³⁶⁸ deposition in such a cell is on the left plot of figure 28.

³⁶⁹ Same as in period 2 most of the neighbouring cells to the underfilled cells are calibrated,
³⁷⁰ except for cell 32 in plane 1, shown on the right of figure 28, which is also affected by the low
³⁷¹ statistics at the edges of the detector.

³⁷² There is a couple of notably faulty FEBs with a different energy response than their neigh-
³⁷³ bours. Besides the expected top half of plane 58, which has about 5× larger response than the

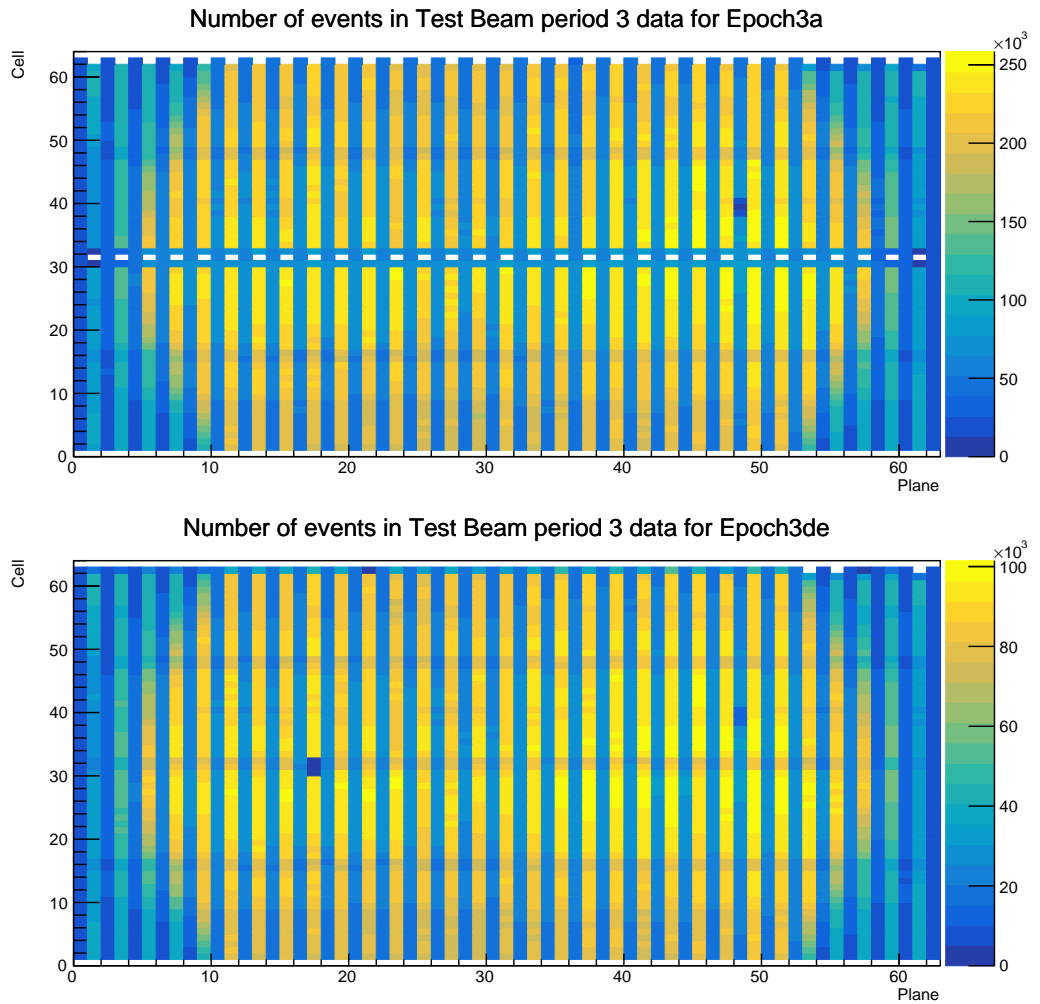


Figure 23: Distribution of events in the period 3 Test Beam data calibration sample. Comparison of Epoch 3a data before the refilling of the underfilled cells and Epoch 3de (combination of Epochs 3d and 3e) after the full refilling.

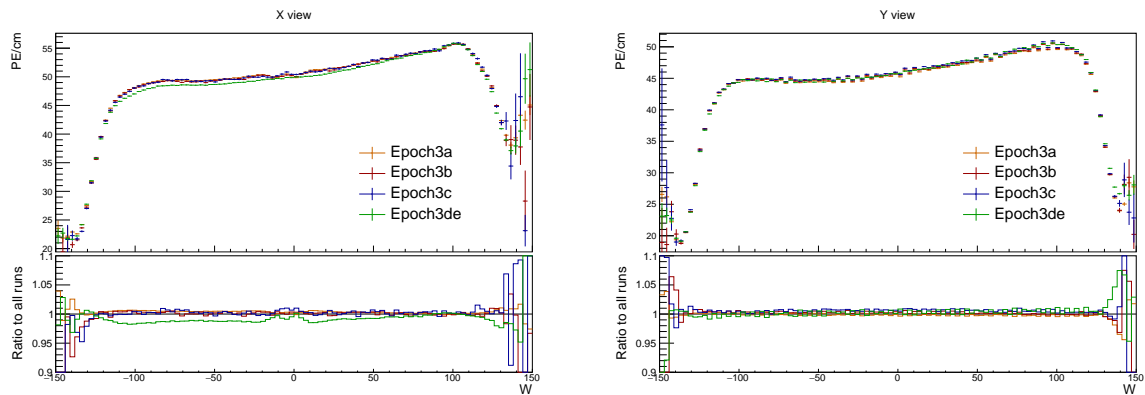


Figure 24: Uncorrected average energy response as a function of the position within a cell (w) for epochs in period 3.

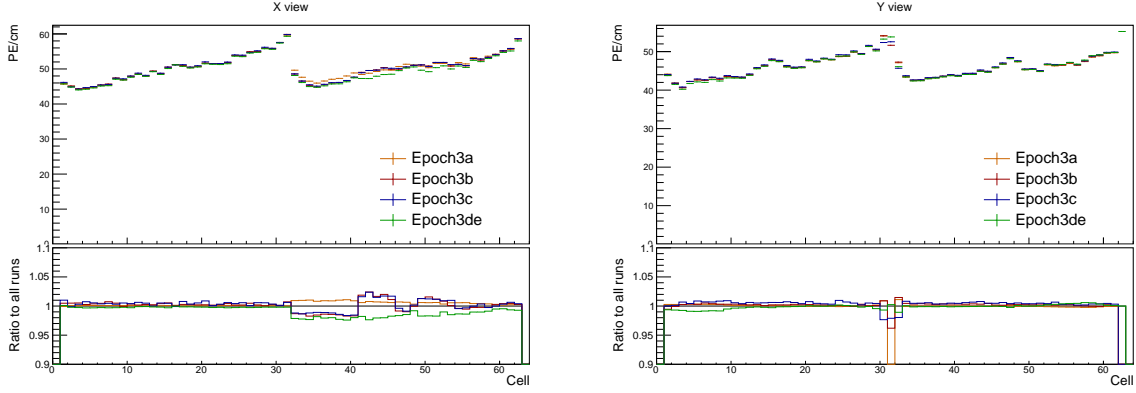


Figure 25: Uncorrected average energy response as a function of cells for epochs in period 3.

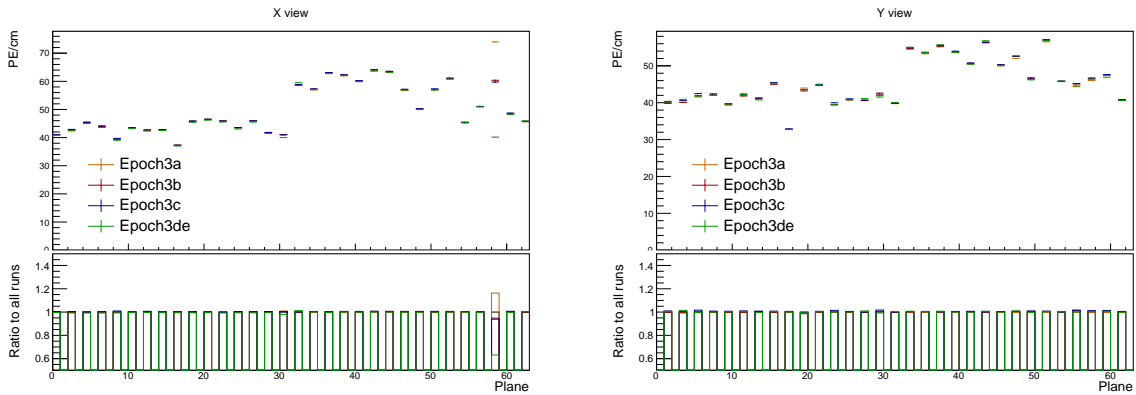


Figure 26: Uncorrected average energy response as a function of planes for epochs in period 3.

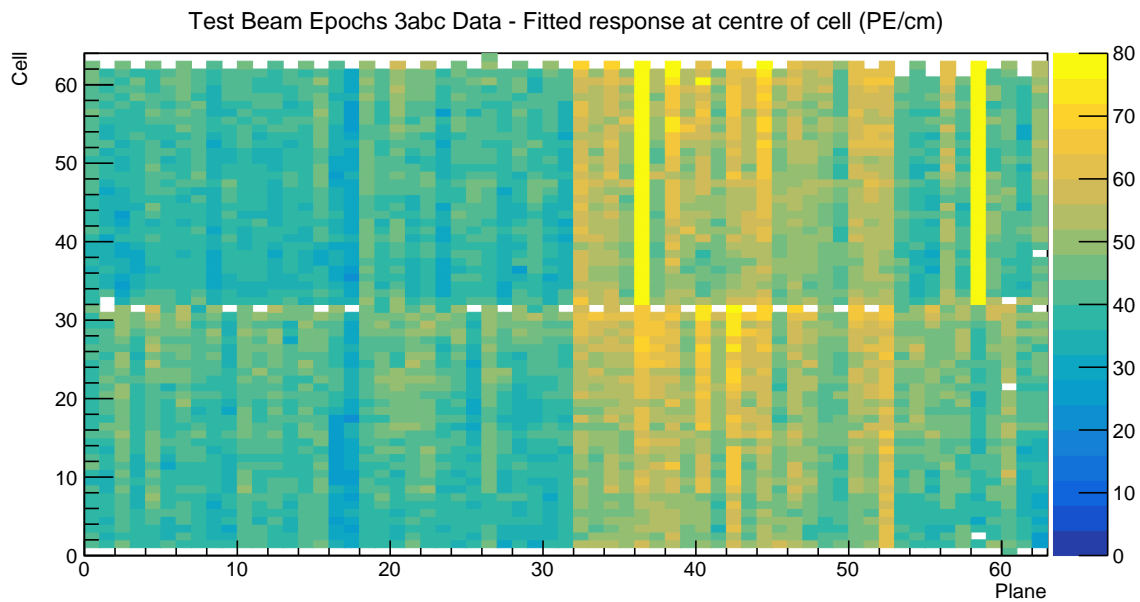


Figure 27: Overview of the relative calibration results for the Test Beam detector period 3, combined epochs 3a, 3b and 3c data. Each cell represents the result of the attenuation fit to the energy response in the centre of that cell. The blank cells are uncalibrated.

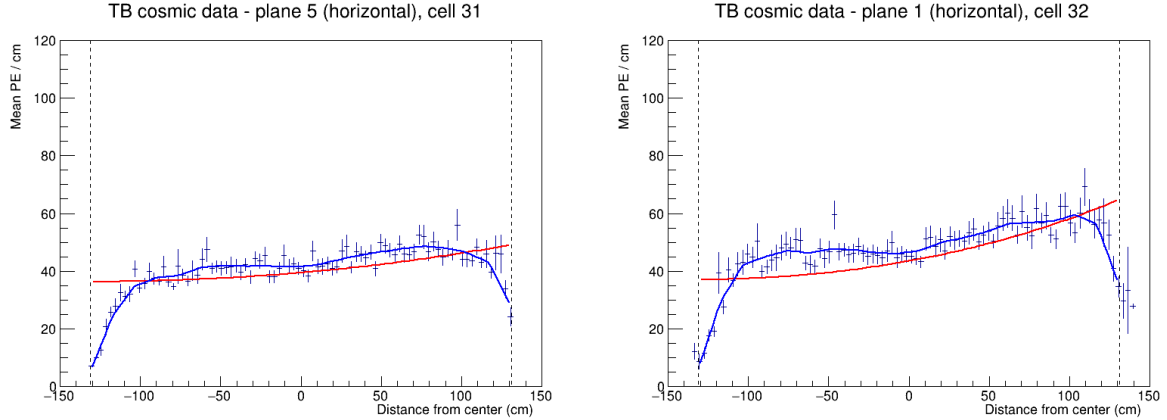


Figure 28: Fit to the energy response in epochs 3 a, b and c. Some underfilled cells that have been refilled in epochs 3b and 3c are now calibrated as shown on the left plot. Cell 32 in plane 1 is the only neighbouring cell to the underfilled cell that didn't manage to get calibrated due to low number of events.

³⁷⁴ usual, it's also the top half of plane 36, which has about $2.5 \times$ larger response as its neighbours.
³⁷⁵ This could mean that the FEB in plane 36 was faulty only for a limited time compared to the
³⁷⁶ FEB in plane 58. The energy deposition for these cells is shown on figure 29.

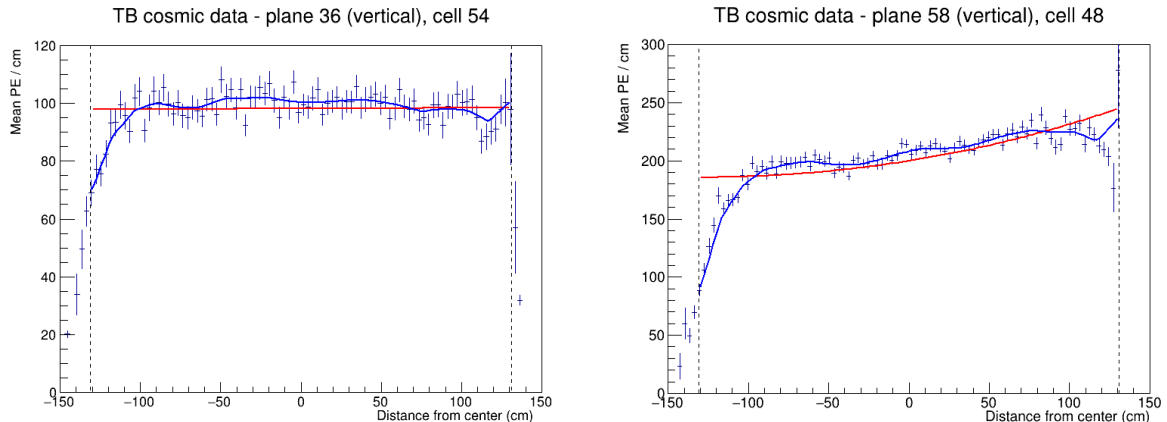


Figure 29: Fit to the energy response in epochs 3 a, b and c. The most obvious faulty FEBs that have a significantly larger energy response than their neighbours.

³⁷⁷ Similarly as in period 2, there are a few cell in the back of the detector that have a sharp
³⁷⁸ rise in the energy response at the edge of the cell, which causes them to be uncalibrated. This
³⁷⁹ can be seen on figure 30.

³⁸⁰ Combined epochs 3d and 3e relative calibration results

³⁸¹ The results of the attenuation fits for epochs 3 d and e are shown on figure 31. There we can
³⁸² see the expected uncalibrated cells in plane 17 related to the dead channel (or possible still
³⁸³ underfilled cell). The energy deposition for this cell and one of its neighbours is shown on
³⁸⁴ figure 32.

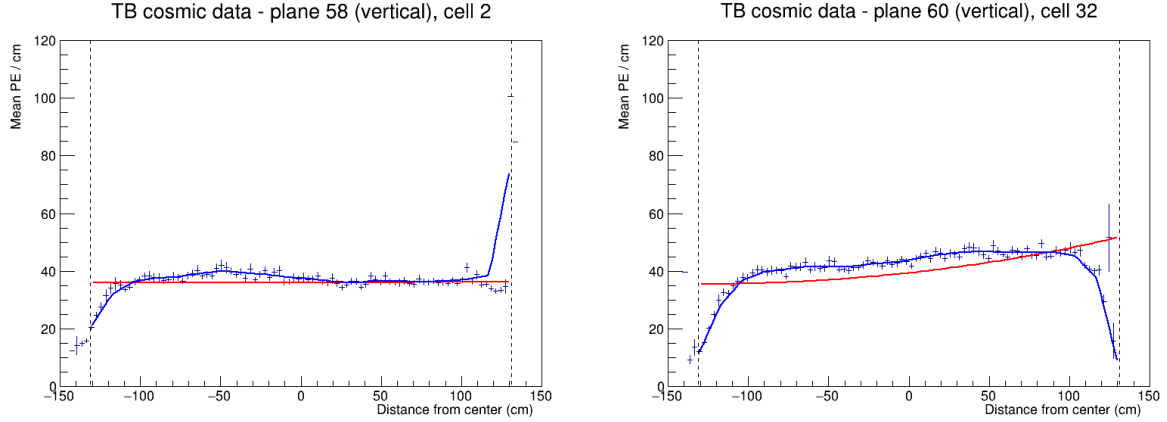


Figure 30: Fit to the energy response in epochs 3 a, b and c. Some cells are not calibrated due to large fluctuations at one edge of the cells.

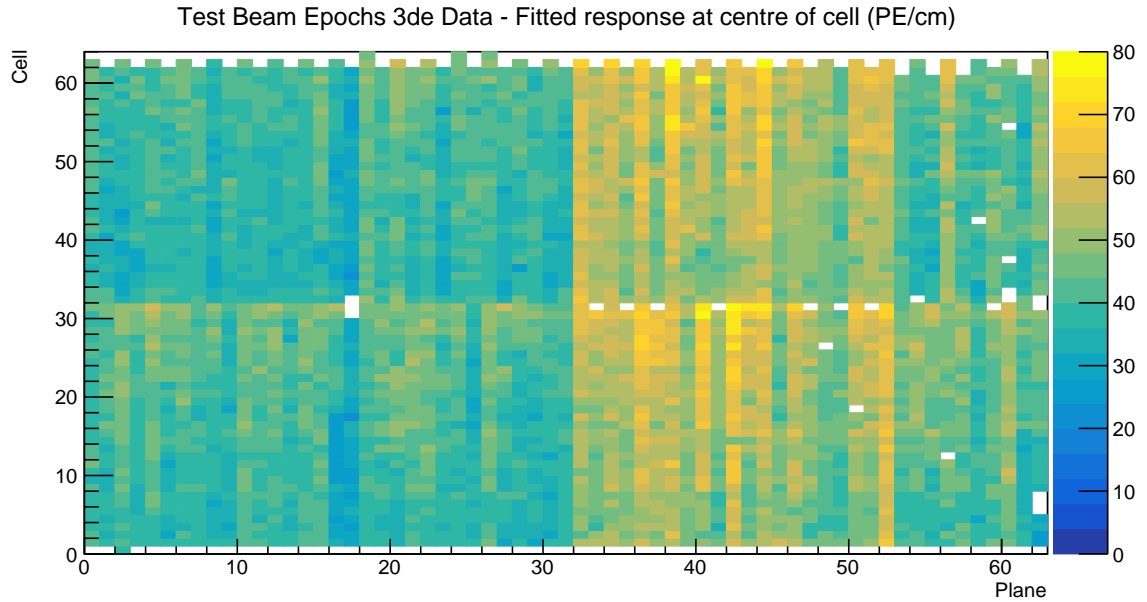


Figure 31: Overview of the relative calibration results for the Test Beam detector period 3, combined epochs 3d and 3e data. Each cell represents the result of the attenuation fit to the energy response in the centre of that cell. The blank cells are uncalibrated.

385 Epochs 3 d and e should have all the previously underfilled cells now refilled, but as can be
 386 seen on figure 31, there's several of these cells that are still uncalibrated. The energy deposition
 387 in these cells is shown on figure 33. We can see that these cells have a fairly large discrepancy
 388 between the left and right side of the cells. This is caused by using different scintillator oils for
 389 the initial filling of the cells and for the refilling. Specifically, these cells have been initially
 390 filled with the Ash River and the Texas oils, which have higher energy depositions compared
 391 to the NDOS oil that was used for the refilling. These oils clearly didn't mix properly which
 392 causes a different energy deposition in different parts of the cells. Since this is a physical effect
 393 that should be accounted for in the calibration and as we can see the fits are actually performing
 394 pretty well and are just confused by the unusual shape. We have therefore decided to manually

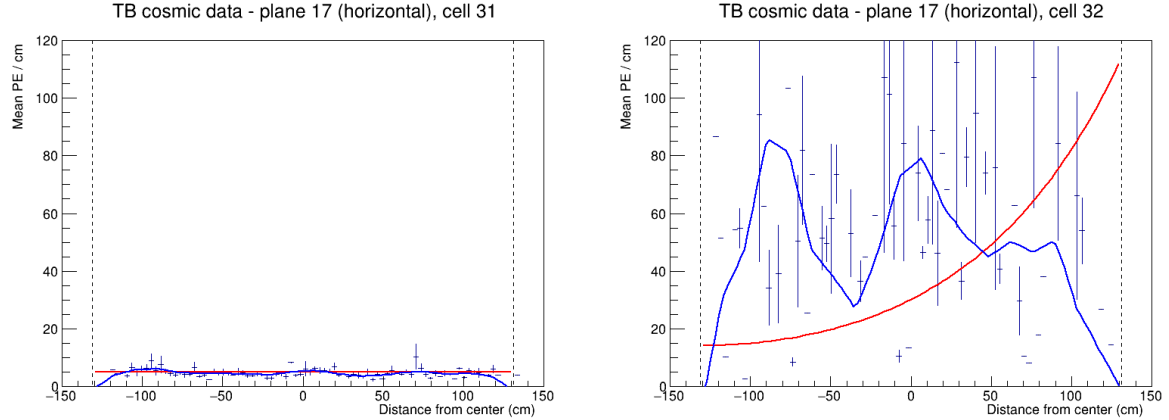


Figure 32: Fit to the energy response in epochs 3 d and e. Possibly dead channel or still underfilled cell.

395 change the χ^2 inside the cvs tables (results of the attenuation fits), so that the $\chi^2 < 0.2$ and
396 these cells are considered calibrated.

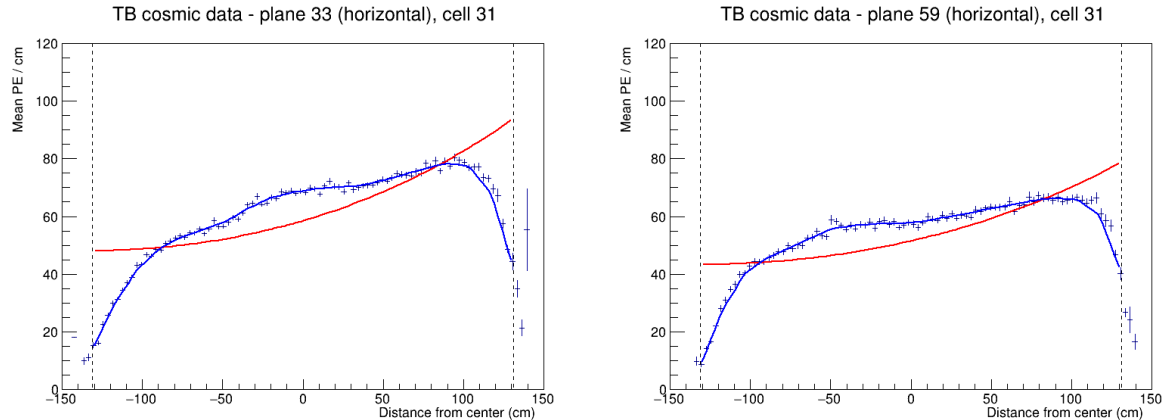


Figure 33: Fit to the energy response in epochs 3 d and e. The scintillator oil used for refilling of the underfilled cells has lower energy response than the oil used for the initial filling. These oils didn't mix properly causing a different energy response in the left and right side of the cell.

397 Some of the cells in the back of the detector have a rise, or drop in energy deposition at the
398 edge of the cell, as can be seen on figure 34. This is similar to the effect seen in period 2 and
399 epochs 3abc and since it's again concentrated in the end of the detector we ignored these cells
400 and left them uncalibrated.

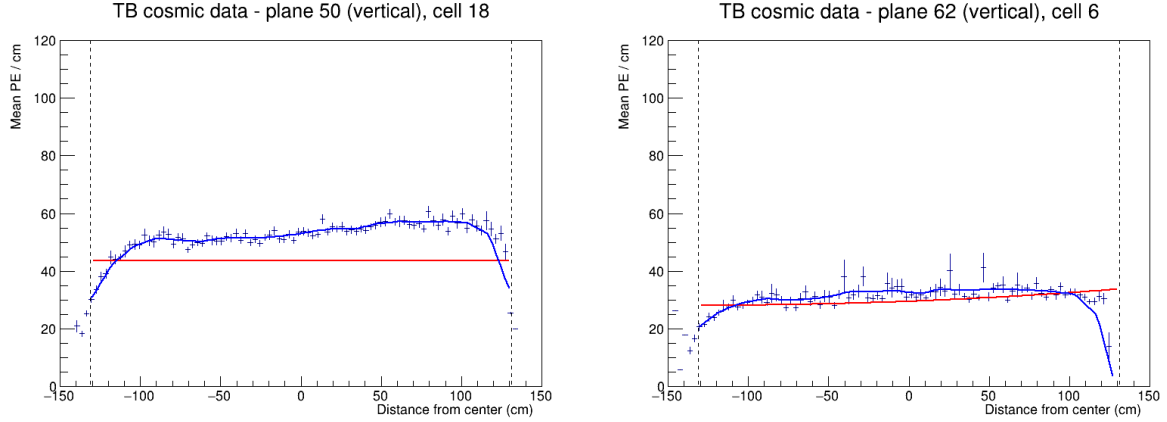


Figure 34: Fit to the energy response in epochs 3 d and e. Some cells have a drop, or a rise of energy response at the edge of the cell. This can be cause by low statistics.

401 4.7 Period 4

402 The period 4 Test Beam data taking period is the best data we managed to collect with almost an
 403 ideal condition of the detector. There's only a few commissioning runs in the very beginning,
 404 which uncovered some dead channels or faulty FEBs that have been fixed. These runs make
 405 epoch 4a shown on the top plot of figure 35.

406 There has also been a cell masking study [reference], during which we masked parts of the
 407 front of the detector to help with FEB saturation. We can clearly see this on the middle plot of
 408 figure 35.

409 Figures 36, 37 and 38 show that the epoch 4a and the cell masking study did have a notice-
 410 able impact on the energy deposition across the detector. We have therefore decided to ignore
 411 these runs and only use the rest of the period 4 data for the calibration.

412 Period 4 relative calibration results

413 Results of the attenuation fits for period 4 are summarised on figure 39.

414 We can see that majority of the detector is calibrated, besides some cells on the edge of the
 415 detector, a few formerly underfilled cells (left plot on figure 40) and one cell with an unusually
 416 high response at the edge of the cell (right plot on figure 40). We treated the formerly underfilled
 417 cells the same way as in epochs 3 d and e, by manually changing their χ^2 to be < 0.2 and
 418 therefore making them calibrated.

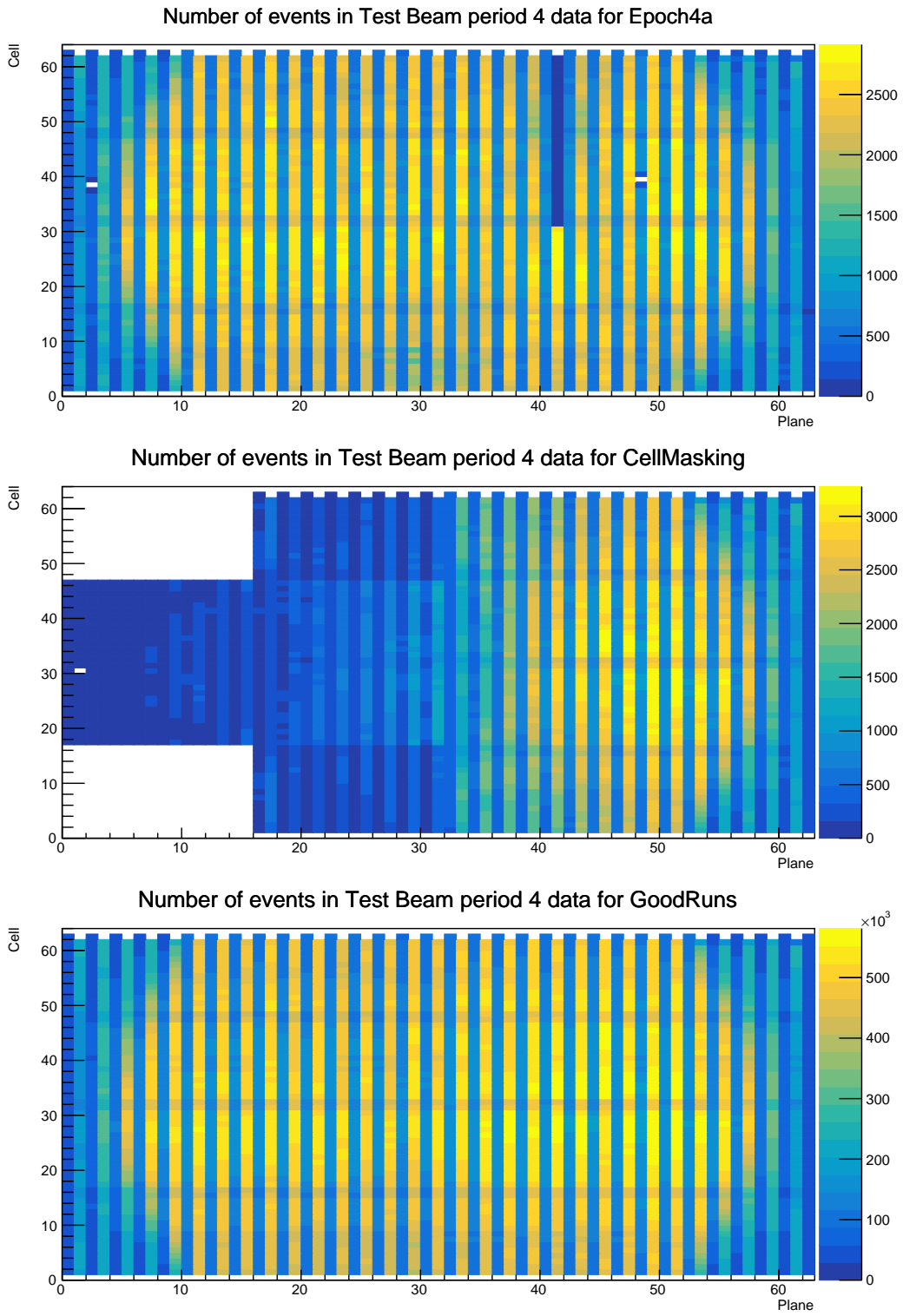


Figure 35: Distribution of events in the Test Beam period 4 data calibration sample. The top plot shows the first three commissioning runs, the middle plot the status of the detector during the Cell Masking studies and the bottom plot shows the rest.

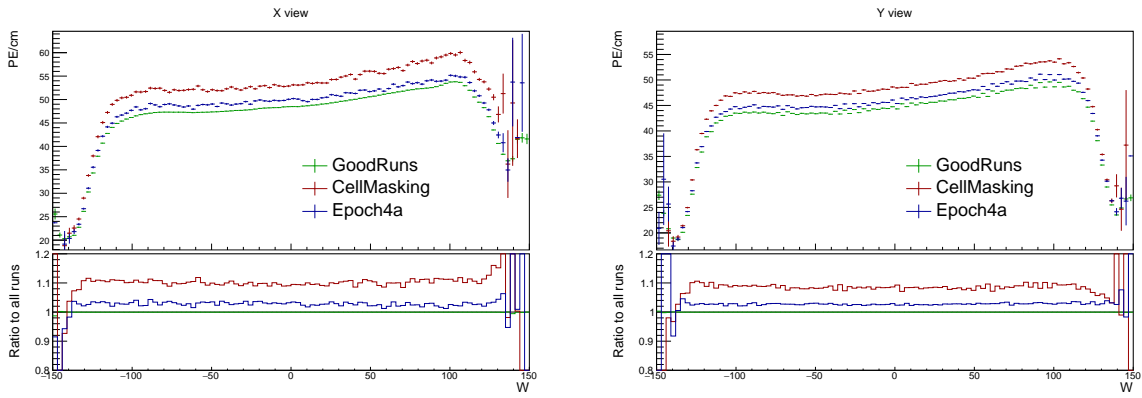


Figure 36: Uncorrected average energy response as a function of the position within a cell (w) for epochs in period 4.

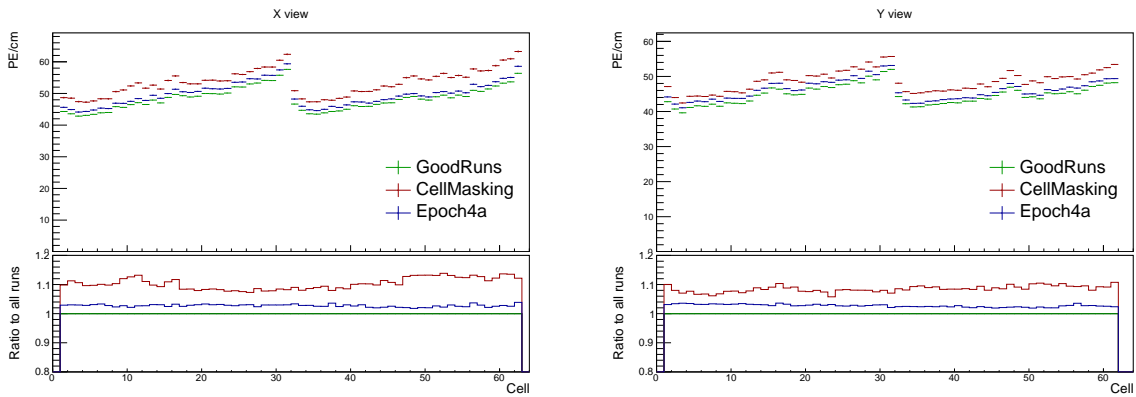


Figure 37: Uncorrected average energy response as a function of cells for epochs in period 4.

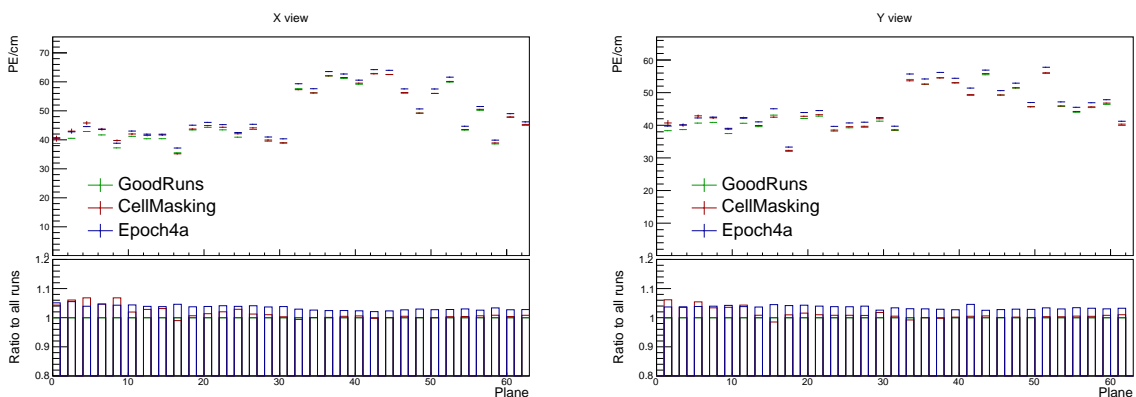


Figure 38: Uncorrected average energy response as a function of planes for epochs in period 4.

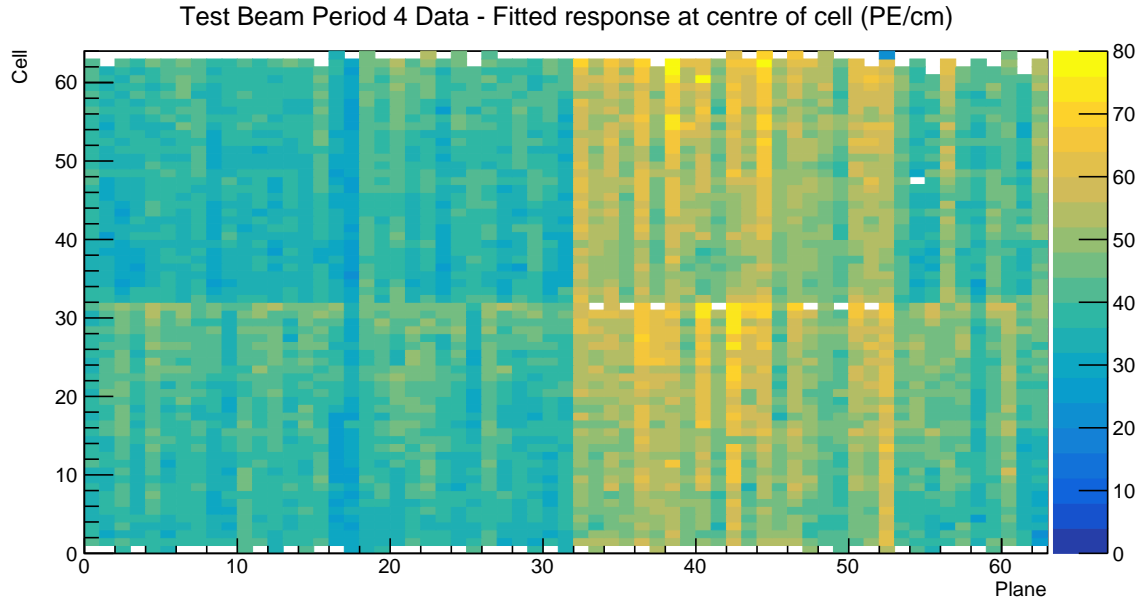


Figure 39: Overview of the relative calibration results for the Test Beam detector period 4 data. Each cell represents the result of the attenuation fit to the energy response in the centre of that cell. The blank cells are uncalibrated.

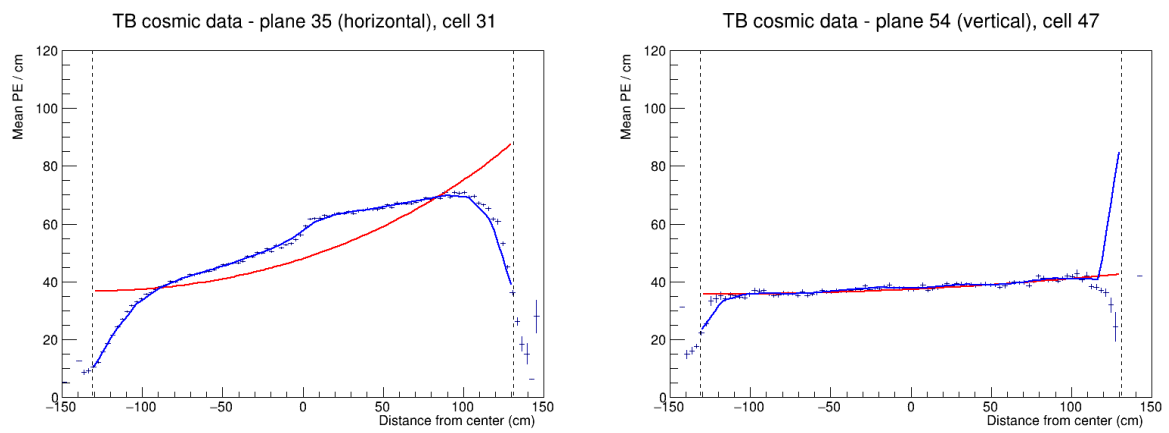


Figure 40: Fit to the energy response in period 4. Previously underfilled cells refilled with a scintillator of a different quality causing an unusual distribution of energy deposition (left). Unusually high energy response at the edge of the cell 47 (right).

⁴¹⁹ **4.8 Absolute calibration results**

⁴²⁰ TO DO: add description of the absolute calibration results, correct the table to fit the page

Sample	NHitsx	MEUx	NHitsy	MEUy	MEU	MEU Err	TrueE/dx	tE/dx Err
epoch 3abc data	2.638e+05	38.49	1.621e+06	39.4	38.94	0.006758	1.772	0.000238
epoch 3de data	1.049e+05	38.63	6.725e+05	39.42	39.02	0.01048	1.772	0.000238
period 2 data	2.322e+05	38.7	1.413e+06	39.4	39.05	0.007252	1.772	0.000238
period 4 data	5.268e+05	38.63	3.316e+06	39.4	39.01	0.004703	1.772	0.000238
simulation	2.829e+05	40.17	1.842e+06	39.93	40.05	0.006418	1.772	0.000238

⁴²¹

⁴²² **4.9 Results**

⁴²³ TO DO: talk about where are the results and what is the final calibration tag

⁴²⁴ **4.10 Validation**

⁴²⁵ TO DO: describe the validation plots and possibly add more plots

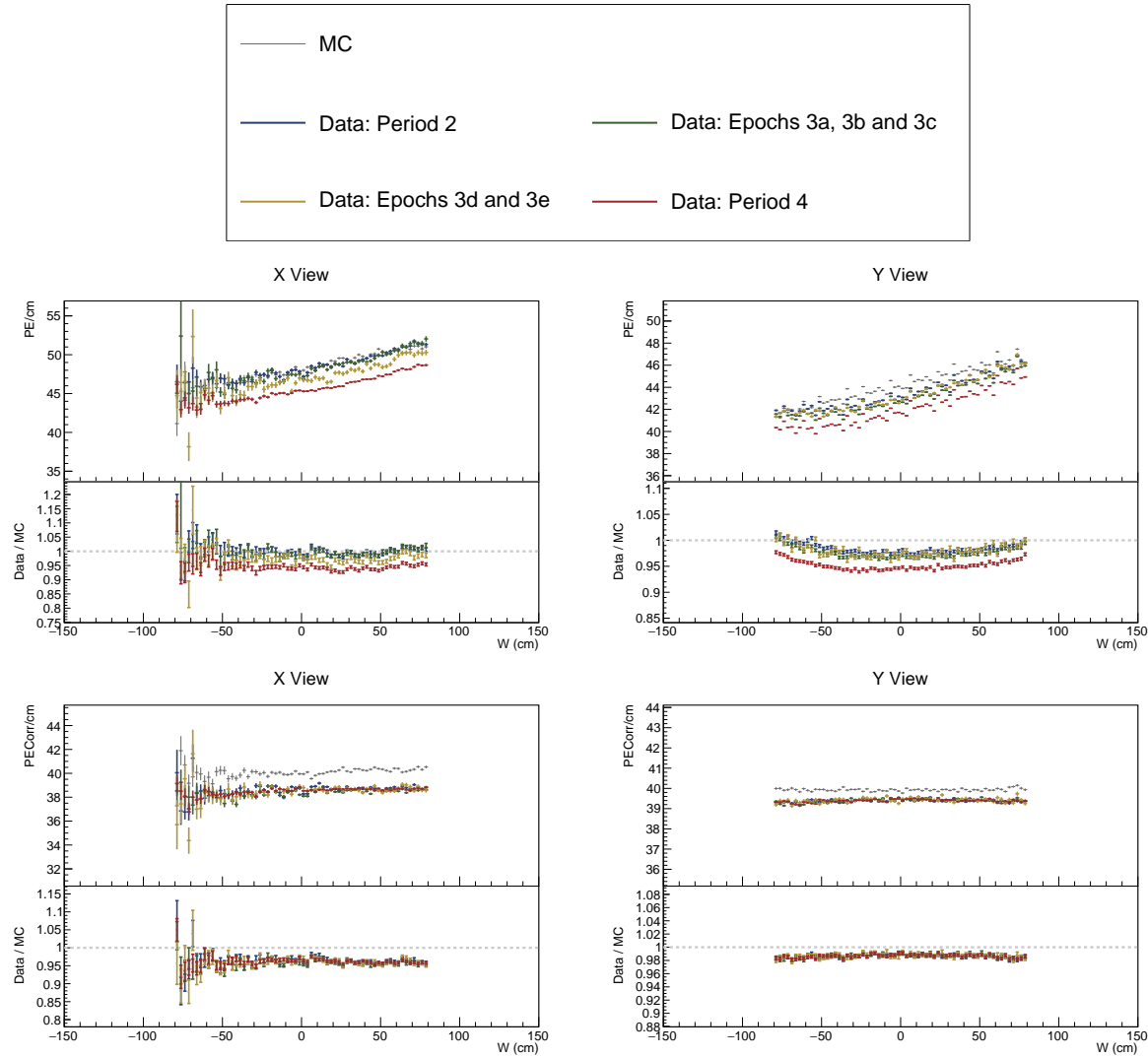


Figure 41: ...

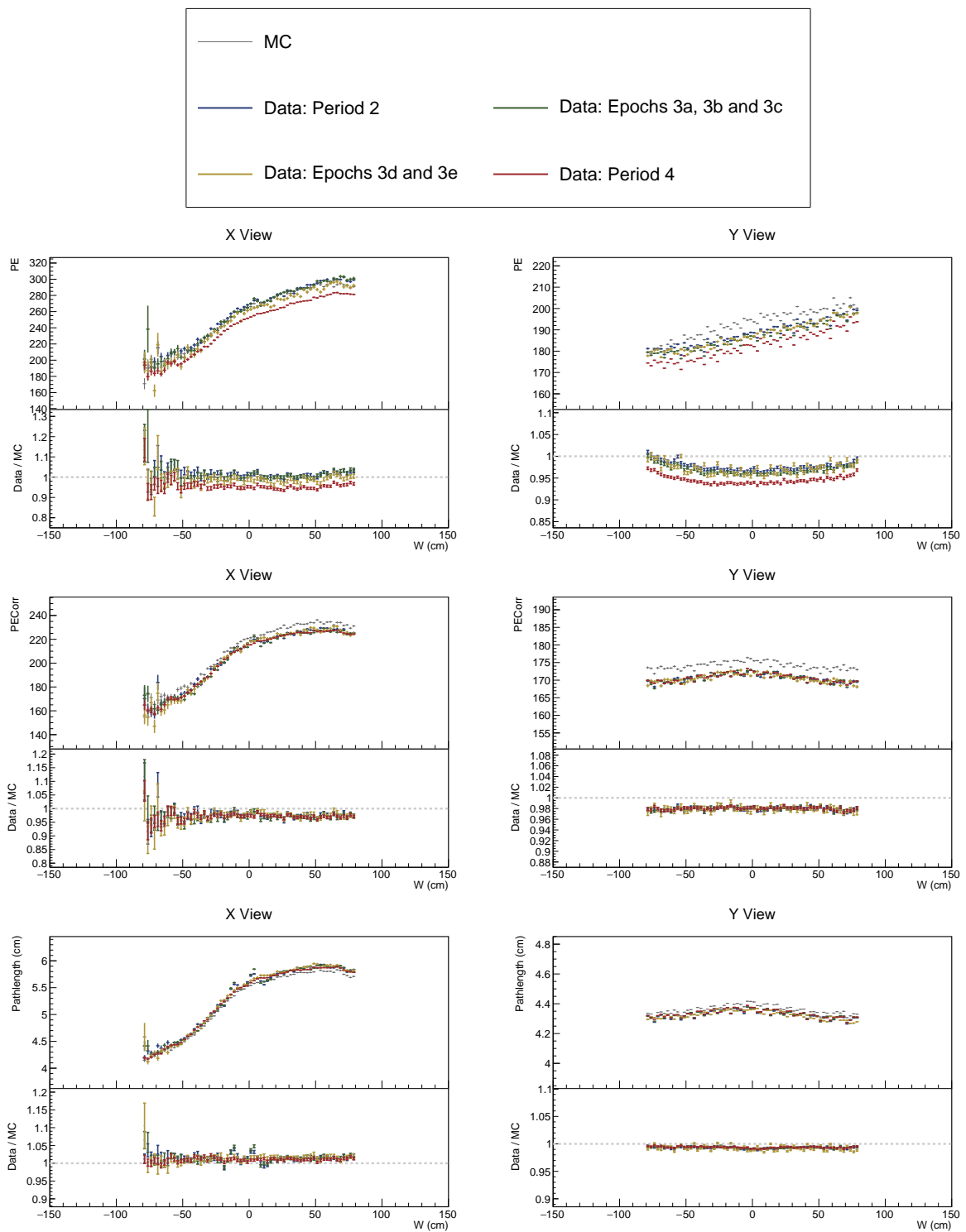


Figure 42: ...

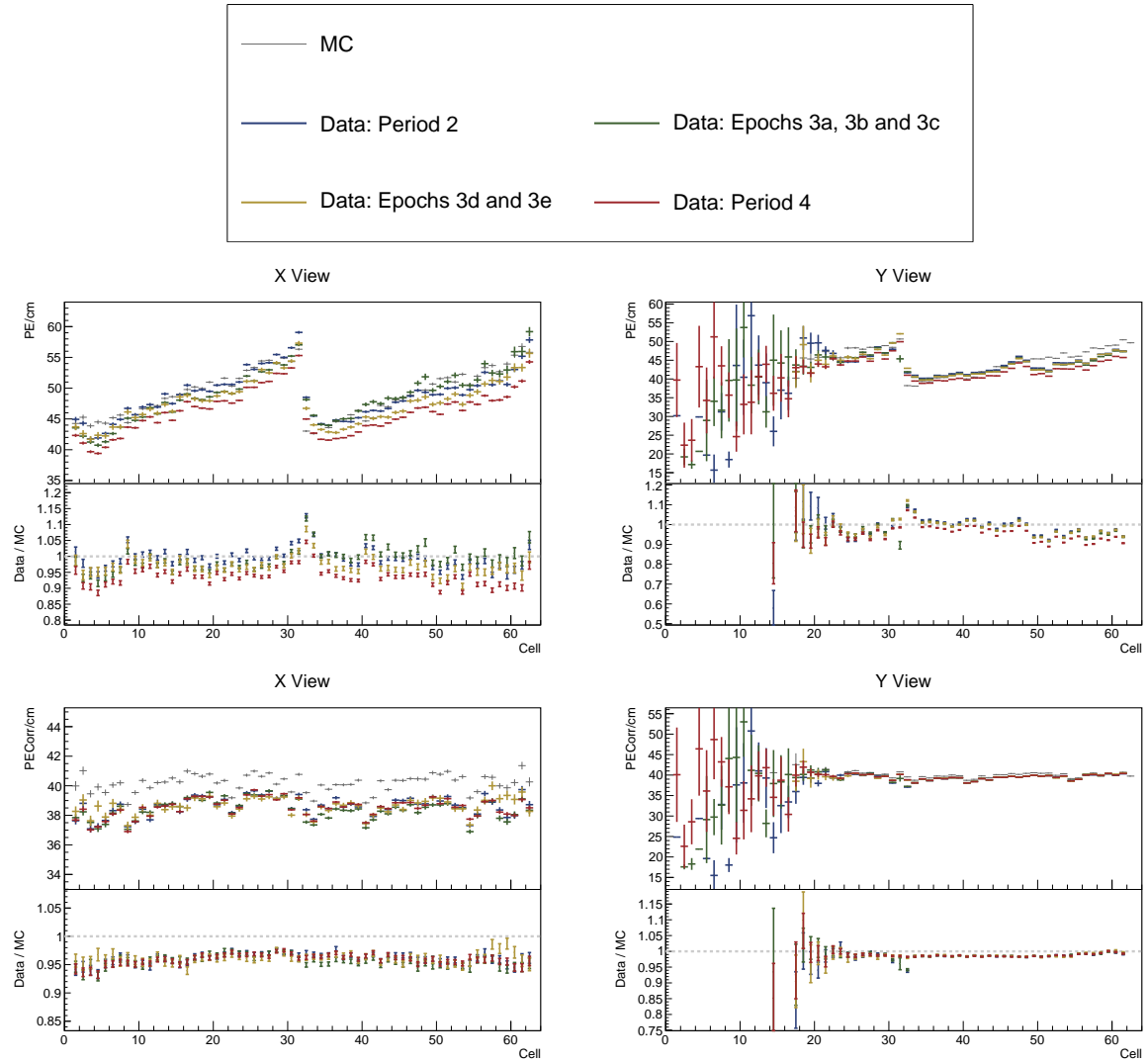


Figure 43: ...

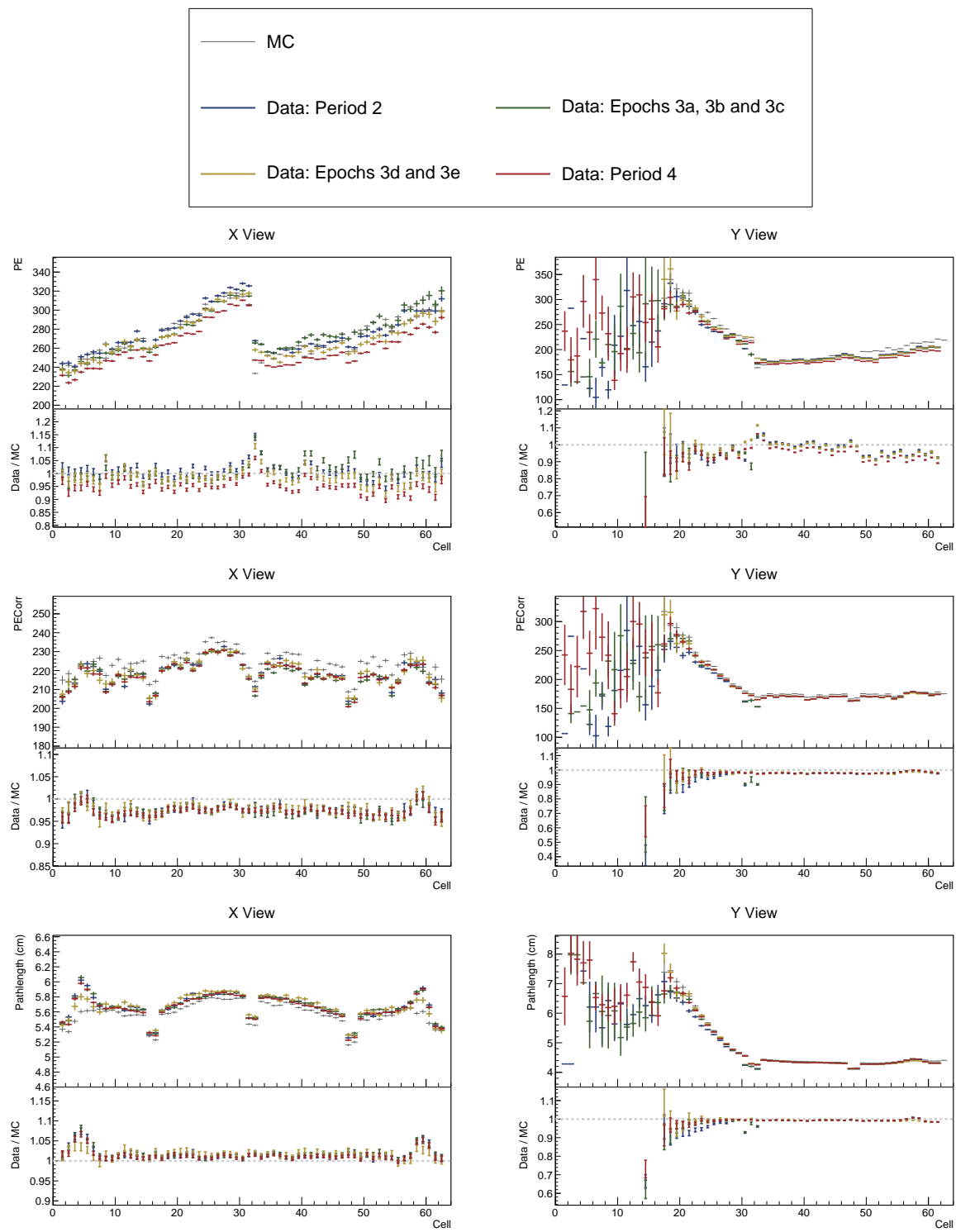


Figure 44: ...

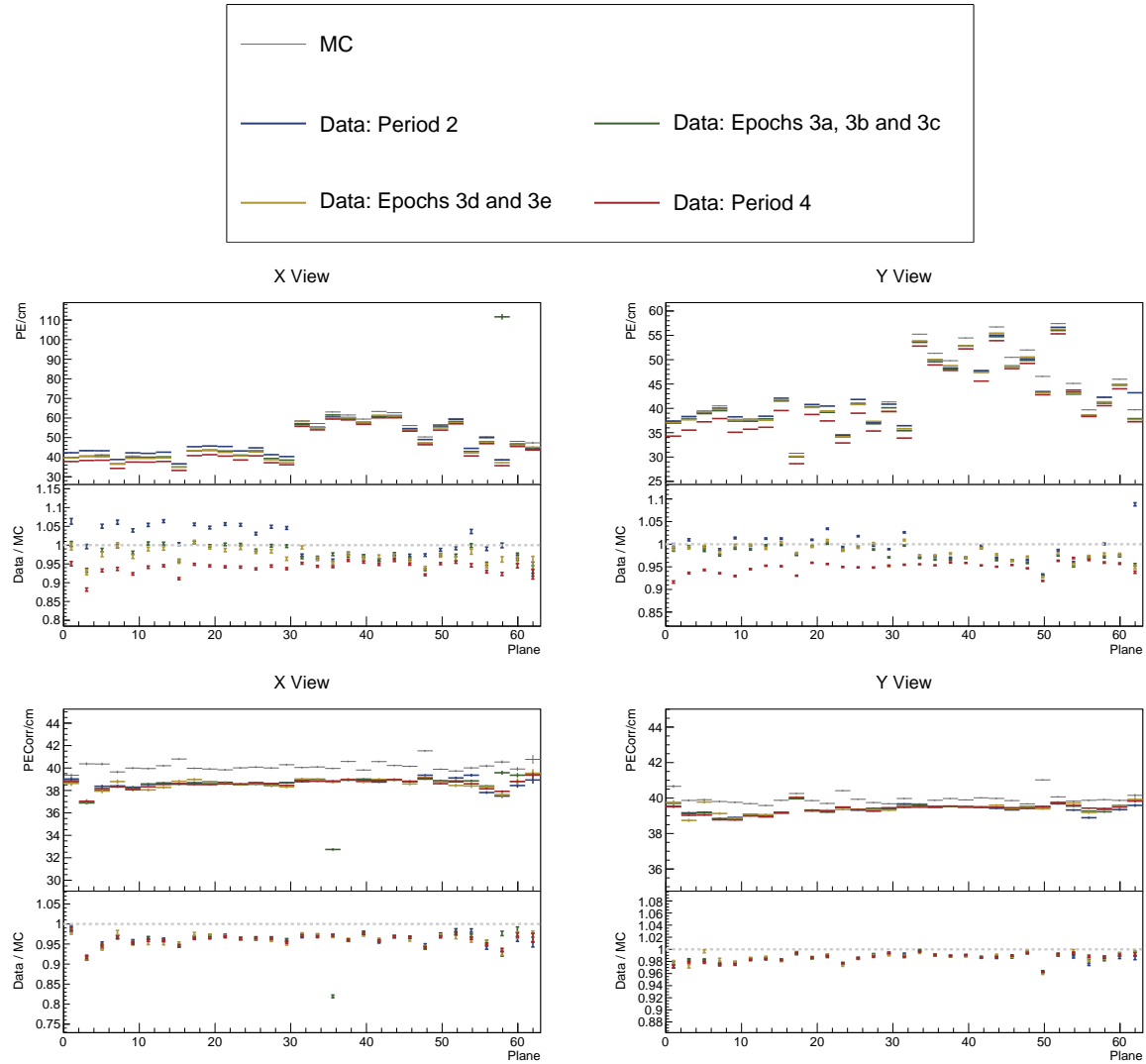


Figure 45: ...

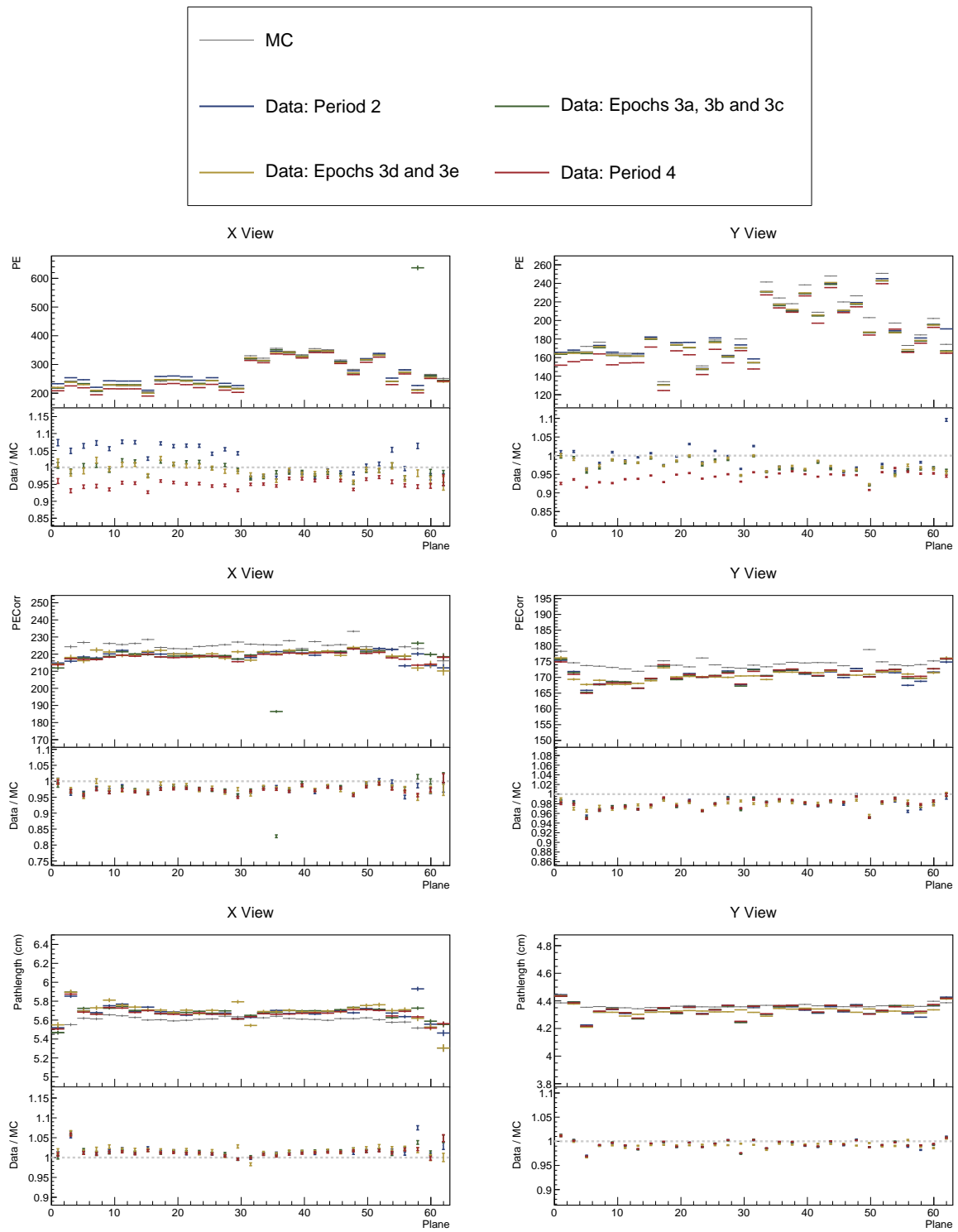


Figure 46: ...

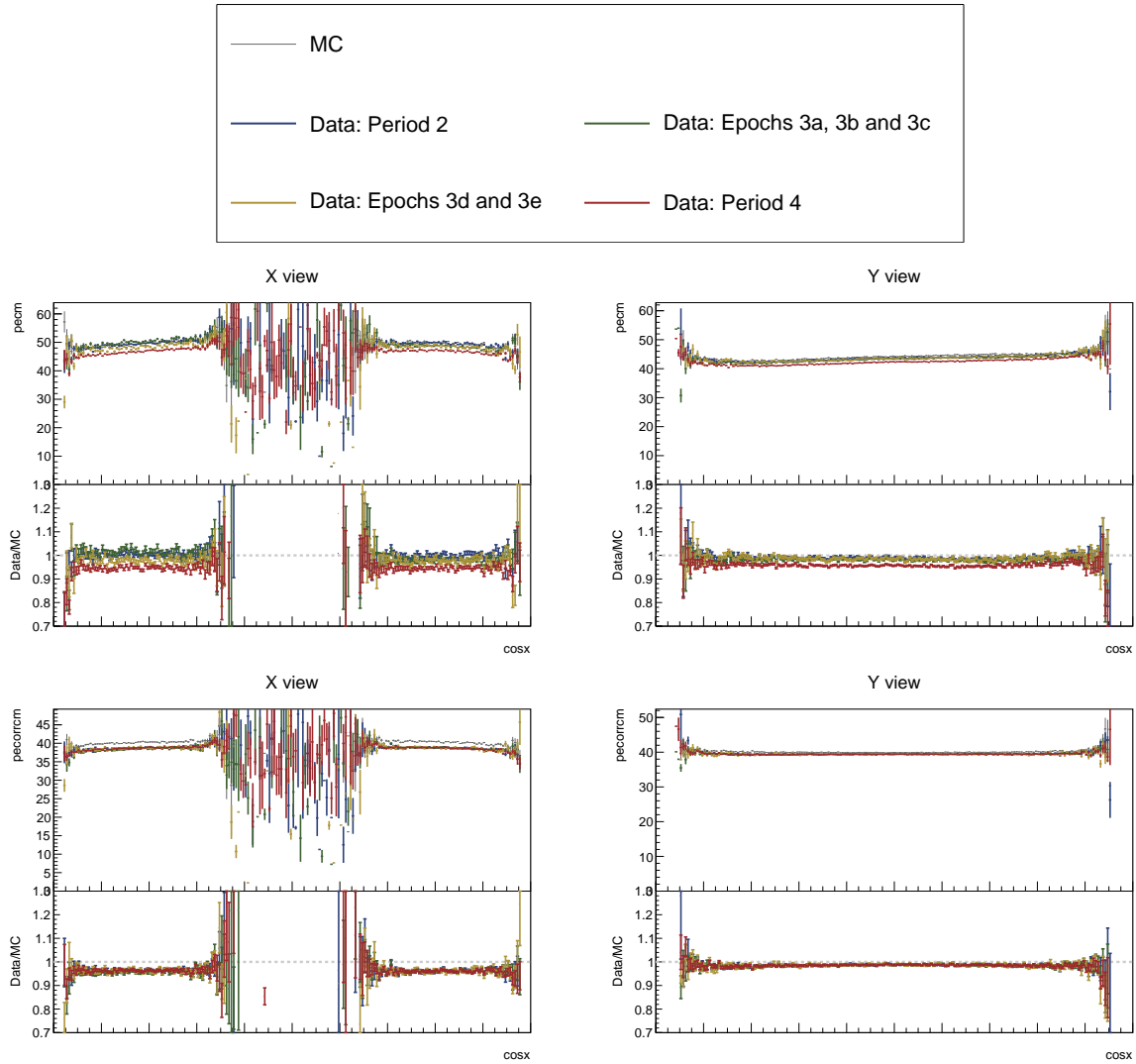


Figure 47: ...

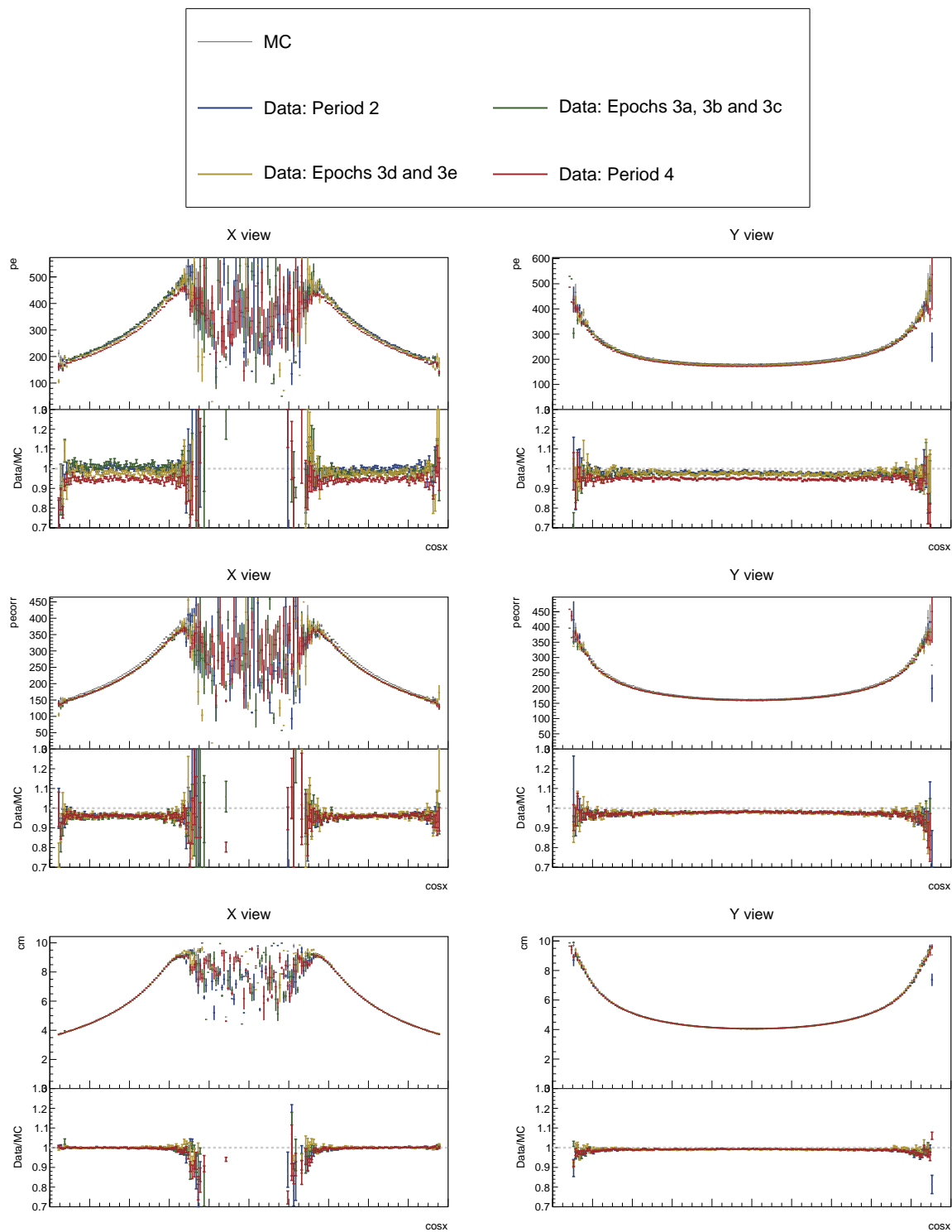


Figure 48: ...

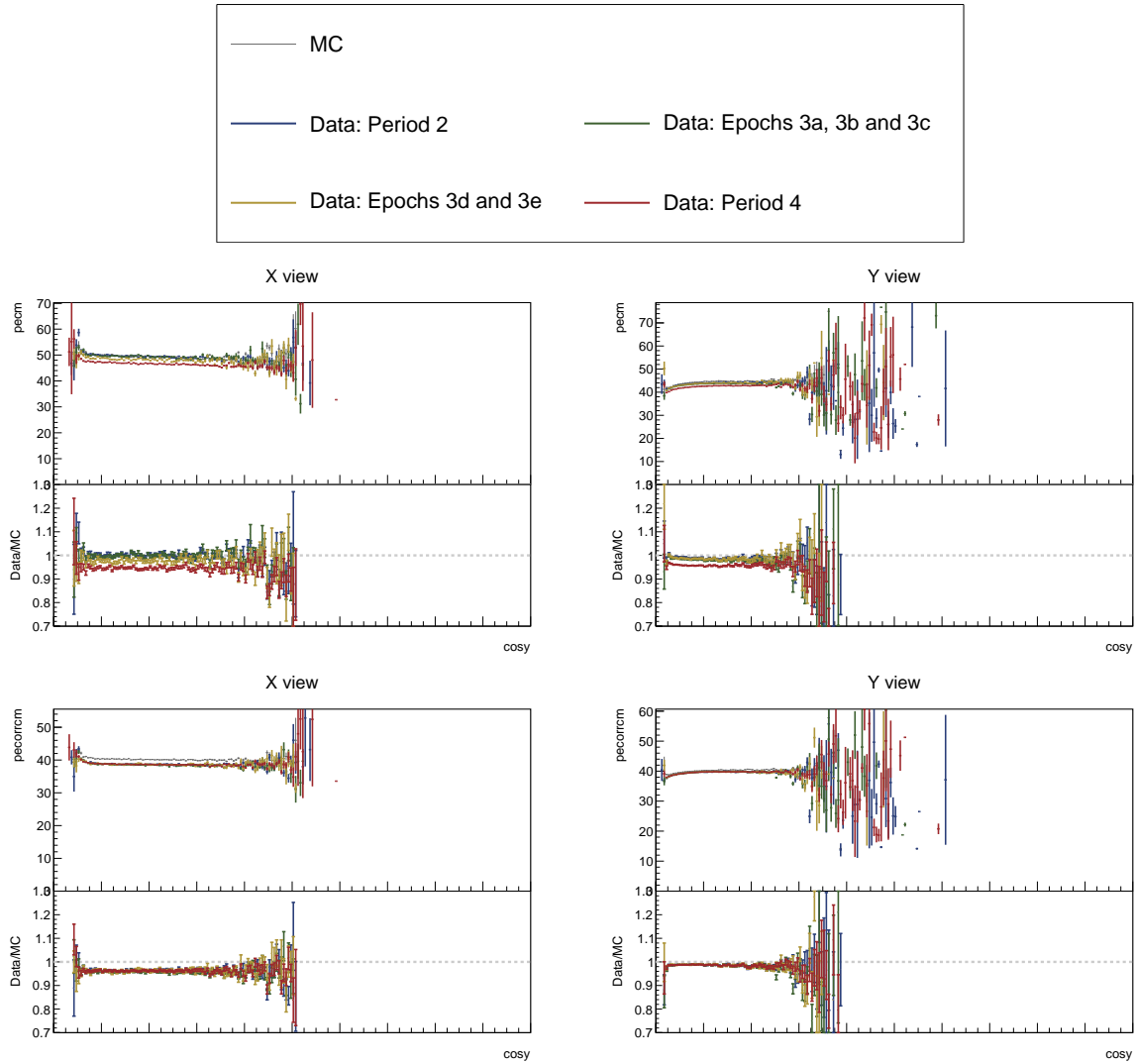


Figure 49: ...

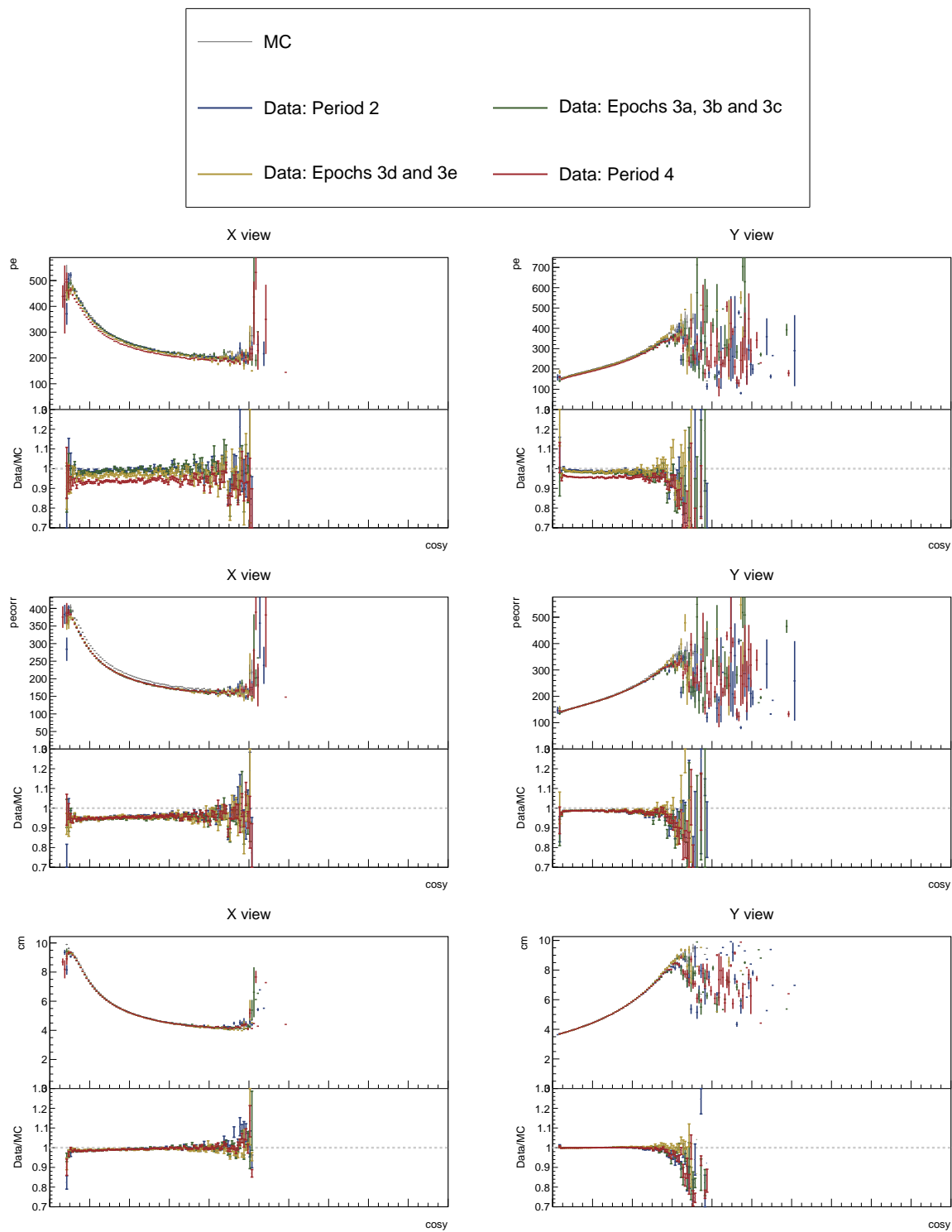


Figure 50: ...

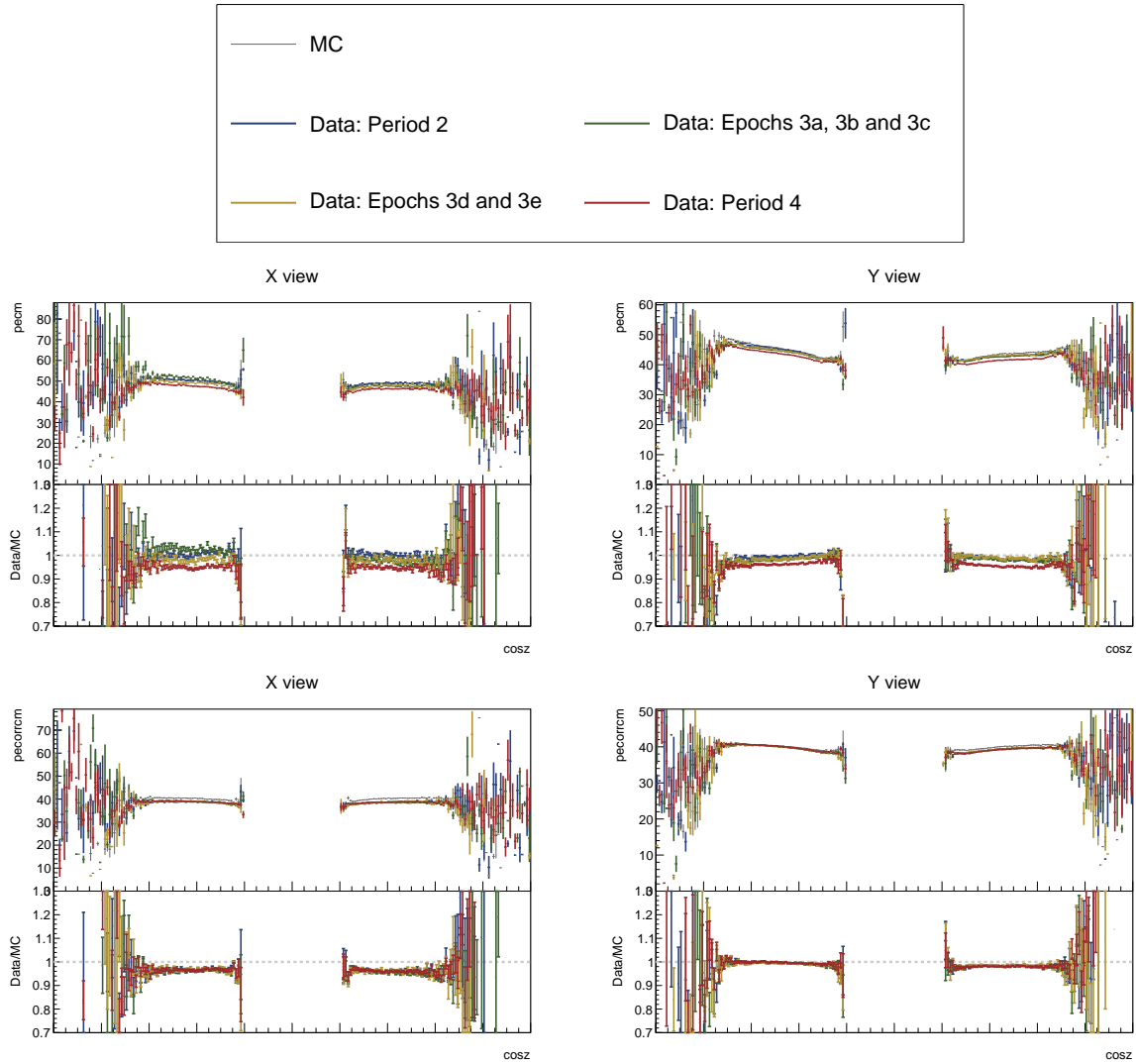


Figure 51: ...

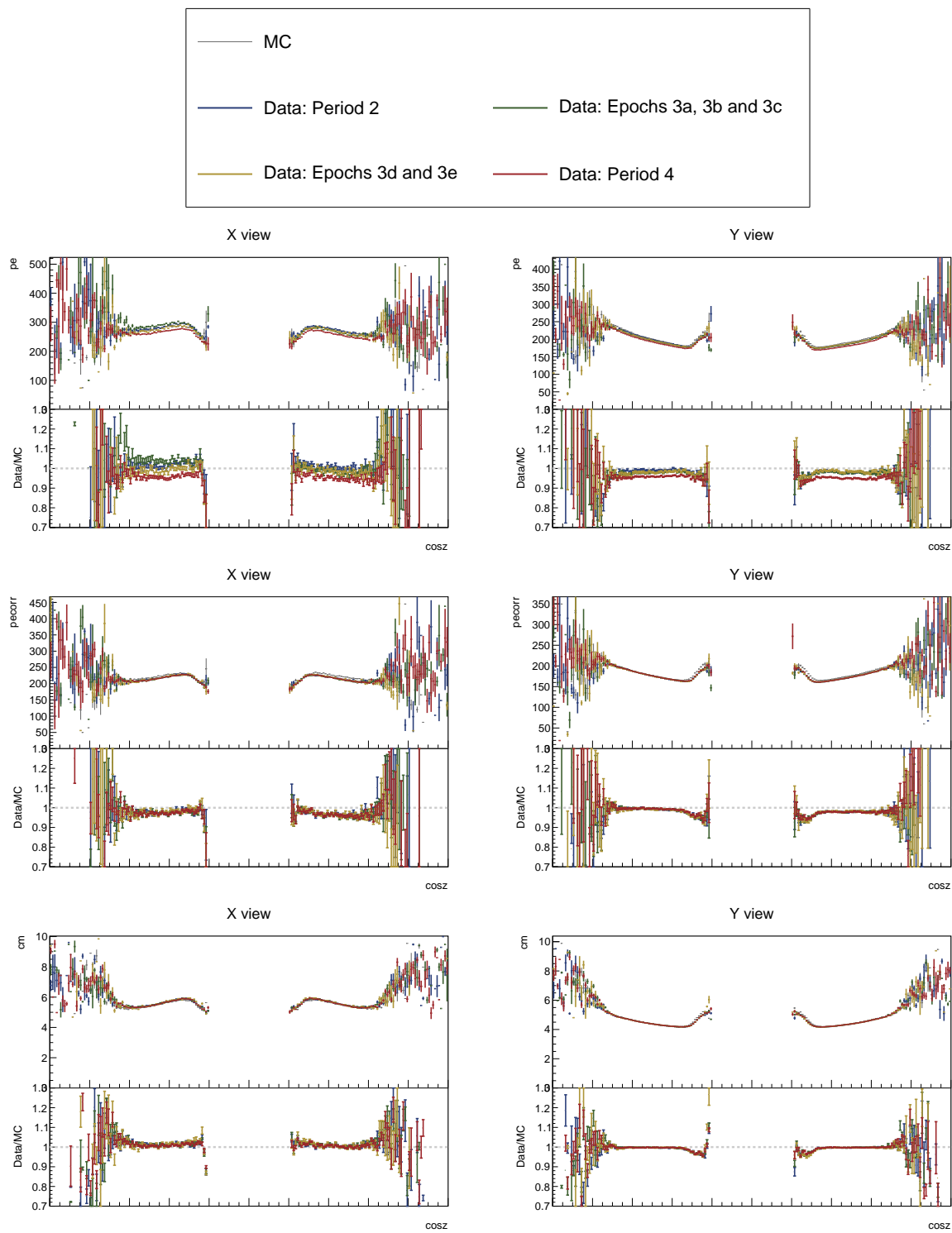


Figure 52: ...

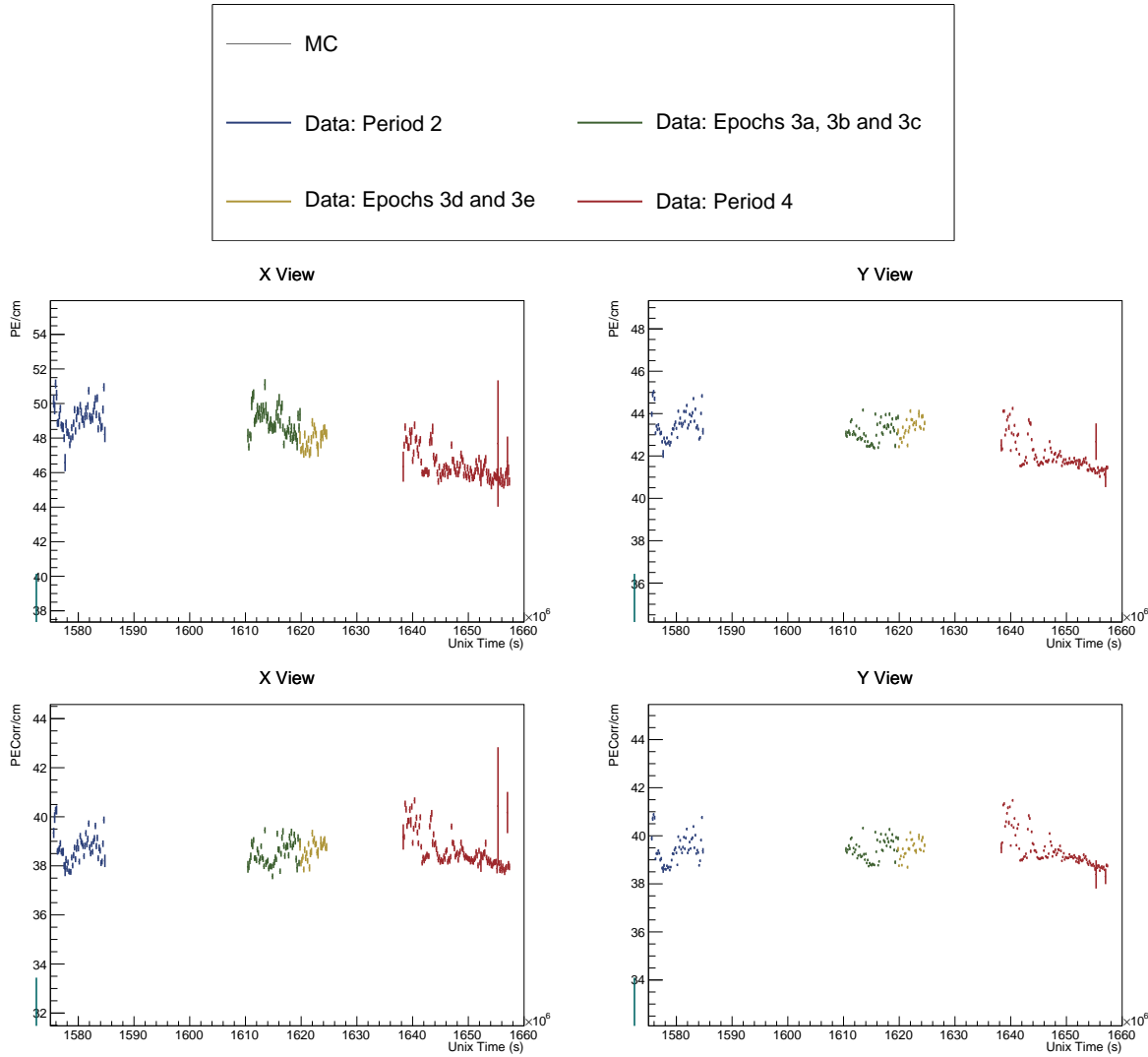


Figure 53: ...

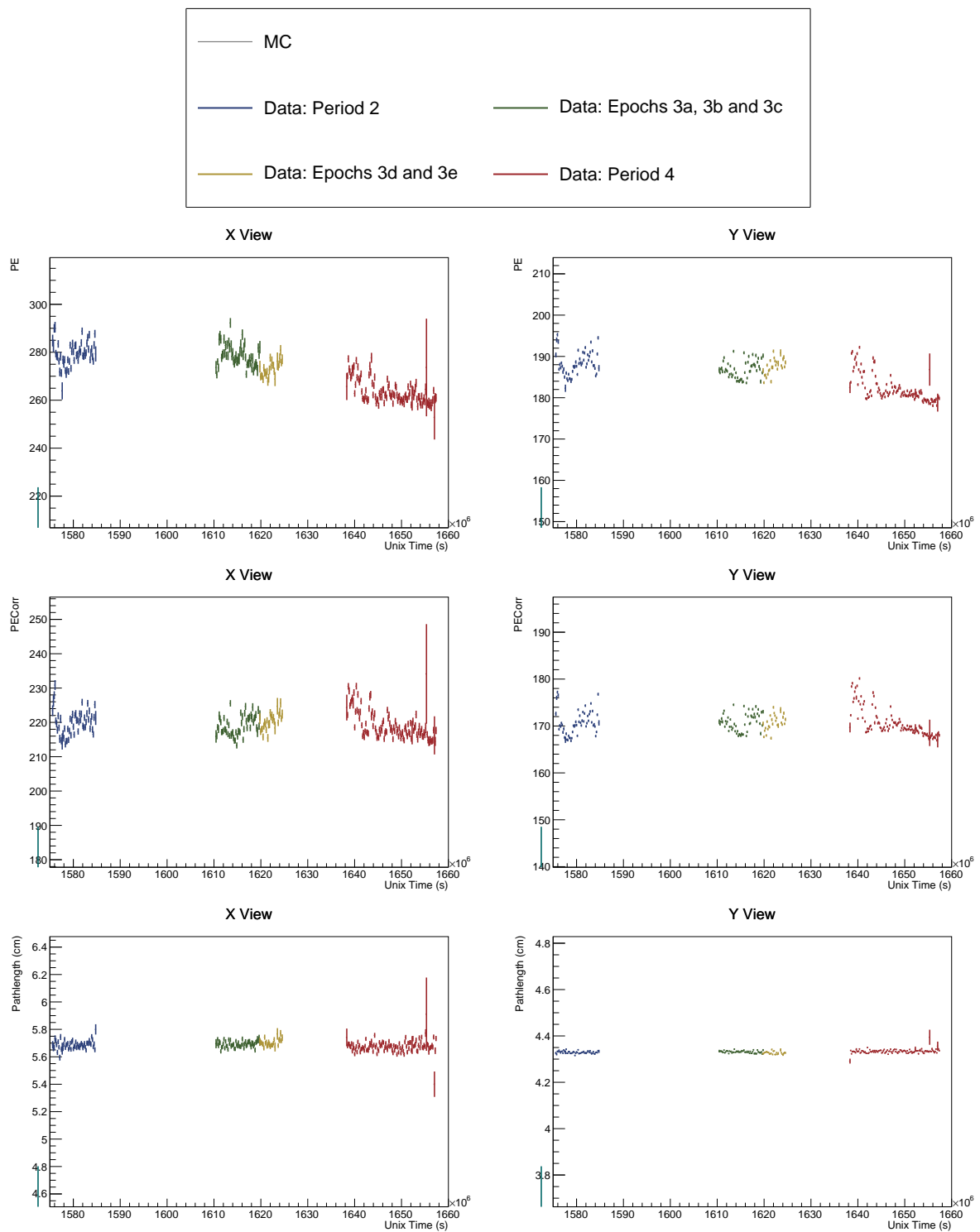


Figure 54: ...

426 **5 Conclusion**

427 TO DO: Write a conclusion

428 **References**

- 429 [1] Alex Sousa. Test Beam Plenary Update - FNAL September 2018. NOVA Document
430 33012, September 2018. NOvA internal document. URL: <https://nova-docdb.fnal.gov/cgi-bin/sso>ShowDocument?docid=33012>.
- 432 [2] Alex Sousa, Ryan Nichol, Karol Lang, and Jeff Nelson. NOvA Test Beam Task Force
433 Report. NOVA Document 15750, August 2016. NOvA technical note. URL: <https://nova-docdb.fnal.gov/cgi-bin/sso>ShowDocument?docid=15750>.
- 435 [3] Kevin Mulder. TB Calibration update. NOVA Document 42700, January 2020.
436 NOvA internal document. URL: <https://nova-docdb.fnal.gov/cgi-bin/sso>ShowDocument?docid=42700>.
- 438 [4] Anna Maureen Hall. TB P2 Calib Update. NOVA Document 50786, June 2021.
439 NOvA internal document. URL: <https://nova-docdb.fnal.gov/cgi-bin/sso>ShowDocument?docid=50786>.
- 441 [5] Robert Kralik. Test Beam calibration results - Spring 2023. NOVA Document 59024, June
442 2023. NOvA internal document. URL: <https://nova-docdb.fnal.gov/cgi-bin/sso>ShowDocument?docid=59024>.
- 444 [6] Alex Sousa. NOvA Test Beam Status and Plans - Support Documentation. NOVA Doc-
445 ument 22172-v2, October 2017. NOvA technical note. URL: <https://nova-docdb.fnal.gov/cgi-bin/sso>ShowDocument?docid=22172>.
- 447 [7] Alex Sousa. NOvA Test Beam Plenary @ IU Collaboration Meeting. NOVA Document
448 29543, May 2018. NOvA internal document. URL: <https://nova-docdb.fnal.gov/cgi-bin/sso>ShowDocument?docid=29543>.
- 450 [8] Michael Wallbank. Final Test Beam Updates (Geometry and Other!). NOVA Document
451 58388, April 2023. NOvA internal document. URL: <https://nova-docdb.fnal.gov/cgi-bin/sso>ShowDocument?docid=58388>.
- 453 [9] Michael Wallbank. Understanding, Improving, Validating the Test Beam Geometry.
454 NOVA Document 57955, February 2023. NOvA internal document. URL: <https://nova-docdb.fnal.gov/cgi-bin/sso>ShowDocument?docid=57955>.
- 456 [10] Robert Kralik. Test beam calibration update. NOVA Document 57516-v2, January
457 2023. NOvA internal document. URL: <https://nova-docdb.fnal.gov/cgi-bin/sso>ShowDocument?docid=57516>.
- 459 [11] Alex Sousa. Test Beam Scintillator Fill Plan. NOVA Document 34196, November
460 2018. NOvA internal document. URL: <https://nova-docdb.fnal.gov/cgi-bin/sso>ShowDocument?docid=34196>.

- 462 [12] Alex Sousa. Test Beam Plenary Update - Jun. 6, 2019. NOVA Document 38349, June
463 2019. NOvA internal document. URL: <https://nova-docdb.fnal.gov/cgi-bin/sso>ShowDocument?docid=38349>.
- 465 [13] Alex Sousa. 2nd Block Filling Status - Nov. 18, 2019. NOVA Document 41961, November
466 2019. NOvA internal document. URL: <https://nova-docdb.fnal.gov/cgi-bin/sso>ShowDocument?docid=41961>.
- 468 [14] Alex Sousa. Filling System and Scintillator Status. NOVA Document 34067, November
469 2018. NOvA internal document. URL: <https://nova-docdb.fnal.gov/cgi-bin/sso>ShowDocument?docid=34067>.
- 471 [15] Junting Huang, Will Flanagan, and Beatriz Tapia Oregui. Test Beam: Light Yield of
472 the Liquid Scintillator Drained from the NDOS Detector. NOVA Document 38740, July
473 2019. NOvA internal document. URL: <https://nova-docdb.fnal.gov/cgi-bin/sso>ShowDocument?docid=38740>.
- 475 [16] Dung Phan. Test Beam: Tintometer Measurement of Texas A&M oil. NOVA Document
476 39088, July 2019. NOvA internal document. URL: <https://nova-docdb.fnal.gov/cgi-bin/sso>ShowDocument?docid=39088>.
- 478 [17] Teresa Megan Lackey. *Proton Scattering in NOvA Test Beam*. PhD thesis, Indiana U.,
479 July 2022.
- 480 [18] David Northacker, Alex Sousa, and Yagmur Torun. Test Beam - Overfilling Horizontal
481 Planes. NOVA Document 49439, March 2021. NOvA internal document. URL: <https://nova-docdb.fnal.gov/cgi-bin/sso>ShowDocument?docid=49439>.
- 483 [19] Keith Matera et al. Calibration Technotes. NOVA Document 13579, January
484 2017. NOvA technical note. URL: <https://nova-docdb.fnal.gov/cgi-bin/sso>ShowDocument?docid=13579>.
- 486 [20] Christopher J. Backhouse. Cell-by-cell attenuation calibration of the NOvA detectors.
487 NOVA Document 7410, December 2014. NOvA technical note. URL: <https://nova-docdb.fnal.gov/cgi-bin/sso>ShowDocument?docid=7410>.
- 489 [21] Evan David Niner. *Observation of Electron Neutrino Appearance in the NuMI Beam with
490 the NOvA Experiment*. PhD thesis, Indiana U., 2015. doi:10.2172/1221353.
- 491 [22] Christopher J. Backhouse. Timing bias introduced by incorrect interpretation of the
492 nanoslice. NOVA Document 13518, June 2015. NOvA technical note. URL: <https://nova-docdb.fnal.gov/cgi-bin/sso>ShowDocument?docid=13518>.
- 494 [23] Luke Vinton. Calorimetric Energy Scale Calibration of the NOvA Detectors. NOVA Doc-
495 ument 13579, document FA_Calorimetric_energy_scale.pdf, July 2015. NOvA technical
496 note. URL: <https://nova-docdb.fnal.gov/cgi-bin/sso>ShowDocument?docid=13579>.
- 498 [24] Keith Matera. Keith's Swell Guide: The Calibration Meta. NOVA Document 13579, doc-
499 ument Calibration_Meta_READFIRST.pdf, January 2017. NOvA technical note. URL:
500 <https://nova-docdb.fnal.gov/cgi-bin/sso>ShowDocument?docid=13579>.

- 501 [25] Christopher Backhouse, Alexender Radovic, and Prabhjot Singh. The Attenuation and
502 Threshold Calibration of the NOvA detectors. NOVA Document 13579, document
503 SA_Attenuation_and_Threshold.pdf, May 2016. NOvA technical note. URL: <https://nova-docdb.fnal.gov/cgi-bin/sso>ShowDocument?docid=13579>.
- 505 [26] Ryan J. Nichol. Fibre brightness from cosmic muon data. NOVA Document 34909, De-
506 cember 2018. NOvA technical note. URL: <https://nova-docdb.fnal.gov/cgi-bin/sso>ShowDocument?docid=34909>.
- 508 [27] Anna Maureen Hall. TB P2 Calib. Summary. NOVA Document 49674, March 2021.
509 NOvA internal document. URL: <https://nova-docdb.fnal.gov/cgi-bin/sso>ShowDocument?docid=49674>.
- 511 [28] Matthew Strait. Update on light level tuning. NOVA Document 43249, February
512 2020. NOvA internal document. URL: <https://nova-docdb.fnal.gov/cgi-bin/sso>ShowDocument?docid=43249>.